J. Fluid Mech. (1997), *vol.* 344, *pp.* 1–41. Printed in the United Kingdom

Nonlinear analysis of convection flow in a tall vertical enclosure under non-Boussinesq conditions

By S. A. SUSLOV AND S. PAOLUCCI

Department of Aerospace and Mechanical Engineering, University of Notre Dame, Notre Dame, IN 46556, USA

(Received 20 July 1996 and in revised form 18 February 1997)

A weakly nonlinear theory, based on the combined amplitude–multiple timescale expansion, is developed for the flow of an arbitrary fluid governed by the low-Mach-number equations. The approach is shown to be different from the one conventionally used for Boussinesq flows. The range of validity of the applied analysis is discussed and shown to be sufficiently large. Results are presented for the natural convection flow of air inside a closed differentially heated tall vertical cavity for a range of temperature differences far beyond the region of validity of the Boussinesq approximation. The issue of possible resonances of two different types is noted. The character of bifurcations for the shear- and buoyancy-driven instabilities and their interaction is investigated in detail. Lastly, the energy transfer mechanisms are analysed in supercritical regimes.

1. Introduction

The classical problem of the flow in a differentially heated vertical cavity of high aspect ratio has attracted the attention of the scientific community for decades. The relatively simple solution of the Boussinesq equations for the basic flow has made this problem the subject of many studies for various conditions (see Suslov & Paolucci 1995*a* for an extensive bibliography). In many practical applications, such as thermal insulation systems in nuclear reactors, the typical temperature differences are of the order of several hundred degrees Kelvin. Thus, neither density nor the other fluid properties variations can be neglected. The attempt to use the conventional Boussinesq approximation for the Navier–Stokes equations for such problems does not lead to a physically correct solution. On the other hand, the low-Mach-number approximation suggested by Paolucci (1982) allows one to take into account arbitrary property variations for a general fluid. Although in the limit of very small temperature differences the low-Mach-number solution recovers the Boussinesq results, the results for any finite temperature variation are quanitatively, the more importantly qualitatively, different (Chenoweth & Paolucci 1985, 1986). In addition, substantial deviations from the Boussinesq results were also found in the linear stability study of convection flows in an enclosure and in a vertical channel (Suslov & Paolucci 1995*a*, *b*) under non-Boussinesq conditions. In these studies it is shown that for any finite temperature difference between the walls the artificial symmetry of the flow obtained using the Boussinesq equations is broken because of property variations. As a result, the instability associated with the shear becomes oscillatory and thus of the Hopf-type rather than the pitchfork-type predicted by the Boussinesq analysis (Mizushima & Gotoh 1983). The second important finding is that at higher values of the temperature difference between the walls a new type of instability which is associated with buoyancy

occurs. This instability is demonstrated to be due to the nonlinear density variation with temperature. The situation is similar to the one found in the Boussinesq limit for large Prandtl numbers ($Pr \gtrsim 12.45$) (Fujimura & Mizushima 1991; Fujimura 1992*a*; Bergholz 1978; Chen & Pearlstein 1989) although the instabilities have a different physical nature.

The weakly nonlinear analysis of the flow in a tall enclosure in the Boussinesq limit shows that the symmetry of the solution is retained even when finite-amplitude disturbances are present (Mizushima & Gotoh 1983). This guarantees that the total mass conservation condition is satisfied automatically. This is not the case when the nonlinear density variation is taken into account: the developing disturbances are not symmetric anymore and the mass conservation condition is non-trivial in this case. Another complication arising in the non-Boussinesq regime is related to the nonlinear property variations. In contrast to the Boussinesq equations, the low-Mach-number equations have a nonlinearity higher than quadratic. For this reason we have found it important to present a detailed discussion of the expansion procedure leading to the derivation of the amplitude equation for general non-Boussinesq flows. This is included in Appendix A. Owing to the complicated structure of the expansions, most of the algebra was performed using the computer algebra system Macsyma 419.0 (1995).

In the present work we use a combined amplitude expansion–multiple timescale analysis. The essence of the method is to compute the small-amplitude expansion corresponding to the most unstable eigenmodes in the linear problem for arbitrary values of the temperature difference and the Grashof number. Separating different orders of the disturbance amplitude one obtains a system of linear equations which reveals the possibility of resonance between the mean flow and the infinite-wavelength disturbance (similar to the one arising in Watson's 1960 approach for subcritical flows and discussed by Davey & Nguyen 1971 and resonance between the fundamental and higher harmonics (discussed in detail in Fujimura & Mizushima 1987; Fujimura 1992*b* for the Boussinesq case). Although we discuss when these resonances occur, their detailed analyses are beyond the scope of the present work. However, we note that these resonances can be successfully analysed by the introduction of appropriate resonant disturbance modes in the expansions. In general, this leads to the appearance of an additional slow timescale associated with the resonance interaction, and modifies the final form of the coupled Landau equations (see Fujimura & Mizushima 1987; Fujimura 1992*b* for a discussion).

Our approach is close to Herbert's (1983) method of amplitude expansion. Originally, the derivation of the amplitude equation and evaluation of the first Landau constant was based on the solvability condition applied to the equations at third order in amplitude (Stuart 1960; Watson 1960; Stewartson & Stuart 1971). It was shown, though, that the conventional solvability condition is meaningful only at the marginal stability surface or in regions where the real amplification rate is substantially small (of the order of amplitude squared). When the absolute value of the real amplification rate is large enough the equations at third order are unconditionally solvable so that one cannot obtain the first Landau constant in a standard way. In order to overcome this difficulty Herbert (1983) proposed fixing the disturbance at one particular point within the flow domain. He showed that when the real amplification rate tends to zero the value of a Landau constant so defined approaches the one obtained from the standard solvability condition. On other hand, as noted in Fujimura & Mizushima (1987), for any finite value of the real amplification rate the value of the Landau constant obtained using Herbert's approach depends sensitively on the choice of the point. From this, one

can deduce that the amplitude becomes essentially a function of the spatial location, which contradicts the initial assumption that the disturbance amplitude is a function of time only. In the present work, we show that by applying an appropriate orthogonality condition, one can remove this inconsistency completely and for a given normalization of linearized eigenfunctions obtain the Landau constant uniquely regardless of the magnitude of the real amplification rate.

In the following sections we formulate the physical problem, discuss the form of the appropriate expansions and equations arising at different orders of amplitude, define the first Landau constant using the orthogonality condition, and derive the Landau equation for the disturbance amplitude. We then discuss the range of validity of the proposed analysis and present the results of the nonlinear non-Boussinesq convection in a tall closed cavity as a function of the temperature difference between the vertical walls. Finally, the two-mode interaction in the vicinity of the codimension-2 point is studied using the coupled Landau equations.

2. Problem definition and governing equations

We consider the two-dimensional convection flow in a very tall rectangular cavity of width H. The vertical walls are isothermal and maintained at the different temperatures T_h^* and T_c^* respectively (asterisks denote dimensional quantities). The enclosure is placed into a uniform gravitational field $\boldsymbol{g}$ which is parallel to the vertical walls. Since we are interested primarily in the case of large temperature differences $\Delta T = T_h^* - T_c^* > 0$ the conventional Boussinesq equations are not applicable here and we adopt the low-Mach-number equations (Paolucci 1982; Chenoweth & Paolucci 1986) in order to describe such a flow:

$$\left.\begin{aligned} \rho\left(\frac{\partial u_i}{\partial y} + u_j\frac{\partial u_i}{\partial x_j}\right) &= -\frac{\partial \Pi}{\partial x_i} + \frac{Gr}{2\epsilon}(\rho - 1)\, n_i + \frac{\partial \tau_{ij}}{\partial x_j}, \\ \rho c_p\left(\frac{\partial T}{\partial t} + u_j\frac{\partial T}{\partial x_j}\right) &= \Gamma\beta T\frac{\mathrm{d}P}{\mathrm{d}t} + \frac{1}{Pr}\frac{\partial}{\partial x_j}\left(k\frac{\partial T}{\partial x_j}\right), \\ \frac{\partial \rho}{\partial t} + \frac{\partial \rho u_j}{\partial x_j} &= 0, \end{aligned}\right\} \tag{1}$$

where

$$\tau_{ij} = \mu\left[\left(\frac{\partial u_i}{\partial x_j} + \frac{\partial u_j}{\partial x_i}\right) - \frac{2}{3}\delta_{ij}\frac{\partial u_k}{\partial x_k}\right]. \tag{2}$$

In writing (2) we used Stokes' hypothesis to relate the coefficient of bulk viscosity to the dynamic viscosity. Here $u_i = (u, v)$ and $x_i = (x, y)$ are velocity components and coordinates in the horizontal and vertical directions respectively and $n_i = (0, -1)$ is the unit vector in the direction of gravity. The equations are made non-dimensional by the use of enclosure width H, reference temperature $T_r = (T_h^* + T_c^*)/2$, viscous speed $u_r = \mu_r/(\rho_r H)$, characteristic time $t_r = H/u_r$, initial thermodynamic pressure P_r which would exist in the cavity with a stationary fluid at the reference temperature, and characteristic value of the dynamic pressure $\Pi_r = \rho_r u_r^2$. All properties of the fluid are non-dimensionalized using respective values evaluated at the reference temperature and thermodynamic pressure.

The above system is complemented by the equation of state and property variations:

$$\rho = \rho(P, T), \quad c_p = c_p(P, T), \quad \mu = \mu(P, T), \quad k = k(P, T), \tag{3}$$

where ρ is the fluid density, c_p is the specific heat at constant pressure, μ is the dynamic viscosity, k is the thermal conductivity, and $\beta = (1/\rho)\,(\partial\rho/\partial T)|_P$ is the coefficient of volume expansion, all dependent on the local temperature T and thermodynamic pressure P. Note that the thermodynamic pressure P, which is a function only of time, is an additional unknown arising from the pressure separation which occurs in the low-Mach-number expansion (Paolucci 1982), and the system of equations (1)–(3) is closed by the global mass conservation condition

$$\int_V \rho \, \mathrm{d}V = 1, \tag{4}$$

where V is the cavity volume.

The boundary conditions for the problem are

$$u = v = 0 \quad \text{and} \quad T = 1 \pm \epsilon \quad \text{at} \quad x = 0, 1, \tag{5}$$

where ϵ is defined in (7). In this work we are concerned primarily with the statistically steady flow sufficiently far from the ends of the cavity so that their effects can be neglected. However, since the cavity is closed, the end effects are still felt through condition (4). Furthermore, the no-penetration condition at the ends of the cavity requires a zero mass flux at any horizontal section, and in particular away from the ends. Allowing for periodicity in the vertical direction, this condition can be written as

$$\int_0^1 \left(\frac{1}{\lambda} \int_{y_0 - \lambda/2}^{y_0 + \lambda/2} \rho v \, \mathrm{d}y \right) \mathrm{d}x = 0, \tag{6}$$

where y_0 is an arbitrary vertical location far enough from the ends and λ is the wavelength. This condition will be seen to lead to the appearance of a uniform vertical pressure gradient whenever the temperature difference between the walls is finite and the flow loses symmetry due to property variations. Note that in the Boussinesq limit both the total mass conservation (4) and zero mass flux condition (6) are satisfied automatically due to the symmetry of the problem and subsequently no spatially uniform vertical pressure gradient is induced.

The dimensionless parameters appearing in the problem are respectively the Grashof number, the temperature difference, the Prandtl number, and a measure of fluid resilience:

$$Gr = \frac{\rho_r^2 \beta_r g \Delta T H^3}{\mu_r^2}, \quad \epsilon = \tfrac{1}{2}\beta_r \Delta T, \quad Pr = \frac{\mu_r c_{pr}}{k_r}, \quad \Gamma = \frac{1}{\sigma_r T_r}\left(\frac{\gamma_r - 1}{\gamma_r} \right), \tag{7}$$

where $\sigma = (1/P)\,(\partial P/\partial T)|_\rho$ is the coefficient of tension, and $\gamma = c_p/c_v$ is the ratio of specific heats, all evaluated at the reference temperature.

Most of the analysis is done for an arbitrary fluid. However, in reporting specific numerical results we assume that the working fluid in our problem is air with a reference temperature $T_r = 300$ K. Air is modelled as a calorically perfect gas which obeys the equation of state

$$\rho = P/T, \tag{8}$$

with constant specific heat at constant pressure (see discussion in Suslov & Paolucci 1995*a*)

$$c_p = 1, \tag{9}$$

and the Sutherland laws for transport properties

$$\mu = T^{3/2}\left(\frac{1 + S_\mu}{T + S_\mu} \right), \quad k = T^{3/2}\left(\frac{1 + S_k}{T + S_k} \right), \tag{10}$$

where, according to White (1974), $S_\mu = S^*_\mu/T_r = 0.368$ and $S_k = S^*_k/T_r = 0.648$. We also take $Pr = 0.71$, $\gamma_r = 7/5$, and (since it follows from the equation of state that $\sigma_r = 1/T_r$) $\Gamma = 2/7$.

It has been shown in Chenoweth & Paolucci (1985) that for a tall enclosure a two-dimensional steady parallel basic flow exists over most of the enclosure far enough away from the top and bottom walls. This flow has been found in Suslov & Paolucci (1995*a*) to be most unstable to two-dimensional infinitesimal disturbances. Since the linear stability analysis predicts no three-dimensionality for the flow in an enclosure of infinite transverse aspect ratio, in this work we limit ourselves to the analysis of two-dimensional small-amplitude disturbances superimposed on the steady basic flow. More detailed discussions of the governing equations, the basic flow solution, and its linear stability are given in Chenoweth & Paolucci (1985, 1986) and Suslov & Paolucci (1995*a*).

3. Expansion procedure

The system of Boussinesq equations conventionally used in convection problems has a quadratic nonlinearity. In contrast, the character of the nonlinearity in the non-Boussinesq system (1)–(6) is much more complicated owing to nonlinear properties variations. For this reason we find it useful to derive rigorously the form of the expansion which is needed for the weakly nonlinear analysis.

Assuming periodicity in the vertical direction, we look for the solution of system (1)–(6) in the Fourier-decomposed form

$$\boldsymbol{W}(t,x,y) = \sum_{m=0}^{\infty} \sum_{n=-\infty}^{\infty} \varepsilon^m \boldsymbol{w}_{mn}(t,x;y)\, E^n(y), \tag{11}$$

where $\boldsymbol{W} = (u, v, T, \Pi, P)^T$, ε is a formal small real expansion parameter, $\hat{\boldsymbol{w}}_{mn} = (\hat{u}_{mn}(t,x),\ \hat{v}_{mn}(t,x),\ \hat{T}_{mn}(t,x)\,\hat{\Pi}_{mn}(t,x;\delta_{0n}\,y),\ \delta_{0n}\,\hat{P}_{mn}(t))^T$, $E = \exp(\mathrm{i}\alpha y)$, and α is a real wavenumber. We note that $E^{-1} = E^*$, where the asterisk denotes the complex conjugate, and, consequently, $\hat{\boldsymbol{w}}_{m-n} = \hat{\boldsymbol{w}}^*_{mn}$ for our solution $\boldsymbol{W}$ to be real. Note also that the dynamic pressure terms must depend on y in order to allow for a non-zero average vertical pressure gradient which is necessary to enforce the zero average mass flux condition (6), and that terms $\hat{P}_{mn}$ are functions only of time since the thermodynamic pressure is spatially uniform under low-Mach-number conditions. In the limit $\varepsilon \to 0$ the expansion (11) should reduce to the steady basic flow solution $\boldsymbol{W}_0(x;y) = (0, v_0(x), T_0(x),\ \Pi_0(y), P_0)^T$ (see Suslov & Paolucci 1995*a* for detailed distributions):

$$\boldsymbol{W}_0 = \lim_{\varepsilon \to 0} \boldsymbol{W} = \sum_{n=-\infty}^{\infty} \hat{\boldsymbol{w}}_{0n}\, E^n. \tag{12}$$

Since $\boldsymbol{W}_0$ is uniform in the vertical direction, we must have $\hat{\boldsymbol{w}}_{00} \equiv \boldsymbol{W}_0$ and $\boldsymbol{w}_{0n\neq 0} \equiv 0$.

Terms of order ε ($m = 1$) should give the linear stability results. Thus, the wavenumber α corresponds to the value chosen for the linear problem. We first investigate the nonlinear behaviour of the disturbance associated with this single mode and, subsequently, consider the case when $\hat{\boldsymbol{w}}_{1|n|\neq 1} \equiv 0$. Later in this paper we generalize the analysis for two-mode interactions.

The further derivation of the form of the expansion is quite involved and is given in Appendix A. Truncating the general form of the resulting expansion (A 12) at $m = 3$ and $n = 2$ we obtain

$$u(x,y,t) = u_{00}(x)+\varepsilon^2|A(t)|^2u_{20}(x) + \{[\varepsilon A(t)\,(u_{11}(x)+\varepsilon^2|A(t)|^2u_{31}(x))\,E+\varepsilon^2A^2(t)\,u_{22}(x)\,E^2]+\text{c.c.}\}, \quad (13)$$

$$v(x,y,t) = v_{00}(x)+\varepsilon^2|A(t)|^2v_{20}(x) + \{[\varepsilon A(t)\,(v_{11}(x)+\varepsilon^2|A(t)|^2v_{31}(x))\,E+\varepsilon^2A^2(t)\,v_{22}(x)\,E^2]+\text{c.c.}\}, \quad (14)$$

$$T(x,y,t) = T_{00}(x)+\varepsilon^2|A(t)|^2T_{20}(x) + \{[\varepsilon A(t)\,(T_{11}(x)+\varepsilon^2|A(t)|^2T_{31}+\varepsilon^2A^2(t)\,T_{22}(x)\,E^2]+\text{c.c.}\}, \quad (15)$$

$$\Pi(x,y,t) = \Pi_{00}(x;y)+\varepsilon^2|A(t)|^2\Pi_{20}(x;y) + \{[\varepsilon A(t)\,(\Pi_{11}(x)+\varepsilon^2|A(t)|^2\Pi_{31}(x))\,E+\varepsilon^2A^2(t)\,\Pi_{22}(x)\,E^2]+\text{c.c.}\}, \quad (16)$$

$$P(t) = P_{00}+\varepsilon^2|A(t)|^2P_{20}. \quad (17)$$

Note that since the basic flow is steady and due to separation of variables in (17) P_{00} and P_{20} are necessarily constant.

If we introduce the property vector $\boldsymbol{g} = (\rho, c_p, \mu, k)^T$, then it can be similarly expanded:

$$\boldsymbol{g} = \boldsymbol{g}_{00}(x)+\varepsilon^2|A|^2\boldsymbol{g}_{20}(x)+\{[\varepsilon A(\boldsymbol{g}_{11}(x)+\varepsilon^2|A|^2\boldsymbol{g}_{31}(x))\,E+\varepsilon^2A^2\boldsymbol{g}_{22}(x)\,E^2]+\text{c.c.}\}, \quad (18)$$

where the components of $\boldsymbol{g}_{00}(x) = \boldsymbol{g}_{00}(P_{00}, T_{00}(x))$ correspond to the properties of the basic flow,

$$\left.\begin{aligned} \boldsymbol{g}_{11} &= \boldsymbol{g}_{00T}\,T_{11},\\ \boldsymbol{g}_{20} &= \boldsymbol{g}_{00T}\,T_{20}+\boldsymbol{g}_{00TT}\,|T_{11}|^2+\boldsymbol{g}_{00P}\,P_{20},\\ \boldsymbol{g}_{22} &= \boldsymbol{g}_{00T}\,T_{22}+\tfrac{1}{2}\boldsymbol{g}_{00TT}\,T_{11}^2,\\ \boldsymbol{g}_{31} &= \boldsymbol{g}_{00T}\,T_{31}+\boldsymbol{g}_{00TT}(T_{11}\,T_{20}+T_{11}^*\,T_{22})+\tfrac{1}{2}\boldsymbol{g}_{00TTT}\,T_{11}\,|T_{11}|^2+\boldsymbol{g}_{00TP}\,T_{11}\,P_{20}, \end{aligned}\right\} \quad (19)$$

and each of the subscripts P or T denotes partial differentiation with respect to P_{00} or $T_{00}(x)$ of the corresponding property equation.

Next we introduce multiple timescales $t_0 = t$, $t_1 = \varepsilon t$, …, so that

$$A(t) = A(t_0, t_1, t_2, \ldots) \quad (20)$$

and thus

$$\frac{\mathrm{d}A}{\mathrm{d}t} = \frac{\partial A}{\partial t_0}+\varepsilon\frac{\partial A}{\partial t_1}+\varepsilon^2\frac{\partial A}{\partial t_2}+\ldots. \quad (21)$$

The physical meaning of the multiple timescales will be discussed in §9.1.

If we now substitute the expansions (13)–(18) and (21) into system (1)–(6) we obtain a set of equations corresponding to each order ε^m and mode E^n. Since the equations for ε^mE^n and ε^mE^{-n} are just complex conjugates of each other we limit our consideration to equations for positive values of n.

4. Basic flow

At order ε^0E^0 we recover the basic flow equations

$$\left.\begin{aligned} \partial\Pi_{00}/\partial x &= 0,\\ \mathrm{D}(\mu_{00}\,Dv_{00})-(Gr/2\epsilon)\,(\rho_{00}-1) &= \partial\Pi_{00}/\partial y,\\ \mathrm{D}(k_{00}\,DT_{00}) &= 0,\\ \mathrm{D}(\rho_{00}\,u_{00}) &= 0, \end{aligned}\right\} \quad (22)$$

$$\left.\begin{aligned} &\rho_{00} = \rho_{00}(P_{00}, T_{00}), \quad c_{p00} = c_{p00}(P_{00}, T_{00}), \quad \mu_{00} = \mu_{00}(P_{00}, T_{00}), \quad k_{00} = k_{00}(P_{00}, T_{00}),\\ &\int_0^1 \rho_{00}\,\mathrm{d}x = 1, \quad \int_0^1 \rho_{00}\,v_{00}\,\mathrm{d}x = 0,\\ &u_{00} = v_{00} = 0, \quad T_{00} = 1\pm\epsilon \quad \text{at} \quad x = 0, 1, \end{aligned}\right\} \quad (23)$$

where $\mathrm{D} \equiv \mathrm{d}/\mathrm{d}x$. Since all terms on the left-hand side of (22) are independent of y, we conclude that

$$\partial \Pi_{00}/\partial y = \bar{\Pi}_{00} = \text{const.} \tag{24}$$

Integrating this in conjunction with the first of equations (22) we obtain $\Pi_{00} = \bar{\Pi}_{00} y + \text{const}$. A detailed discussion of the analytical and numerical basic flow solution, and of the necessary conditions for its existence for the specific property variations (8)–(10) is given in Chenoweth & Paolucci (1985, 1986) and Suslov & Paolucci (1995*a*).

5. Linear disturbances

At order $\varepsilon^1 E^1$ we obtain the linear perturbation equations which in matrix form are

$$A\boldsymbol{A}_\alpha \boldsymbol{w}_{11} - \frac{\partial A}{\partial t_0}\boldsymbol{B}\boldsymbol{w}_{11} = 0, \tag{25}$$

where $\boldsymbol{w}_{11} = (u_{11}, v_{11}, T_{11}, \Pi_{11})^T$, $u_{11} = v_{11} = T_{11} = 0$ at $x = 0$ and $x = 1$ and the elements of $\boldsymbol{A}_\alpha$ and $\boldsymbol{B}$ are given in Appendix B. This system of linear differential equations has a solution of the form $A(t)\boldsymbol{w}_{11}$, where $A(t) = \tilde{A}(t_0, t_2, \ldots)\,\mathrm{e}^{\mathrm{i}\sigma^I t_0}$,

$$\partial \tilde{A}/\partial t_0 = \sigma^R \tilde{A}, \tag{26}$$

and $\sigma = \sigma^R + \mathrm{i}\sigma^I$ and $\boldsymbol{w}_{11}$ are respectively the eigenvalue and eigenvector of the generalized eigenvalue problem

$$\mathbf{L}_{\alpha,\sigma}\boldsymbol{w}_{11} = 0, \tag{27}$$

where we find it convenient to define the linear operator $\mathbf{L}_{\alpha,\sigma} \equiv (\boldsymbol{A}_\alpha - \sigma\boldsymbol{B})$ and its adjoint $\mathbf{L}^\dagger_{\alpha,\sigma} \equiv (\boldsymbol{A}^*_\alpha - \sigma^*\boldsymbol{B}^*)^T$ which we will use later. This eigenvalue problem has been solved using the specific property variations (8)–(10) for a wide range of Gr and ϵ in Suslov & Paolucci (1995*a*). Since for our problem $\max|v_{11}| \geqslant \max(|u_{11}|, |T_{11}|)$ we normalize the eigenvectors in such a way that

$$\max_x |v_{11}| = \max_x |v_{00}| \tag{28}$$

so that we can judge the disturbance magnitude by its amplitude only.

The total mass in the enclosure and the average vertical mass flux are not affected at this order owing to periodicity of the disturbance.

For convenience, in subsequent sections we redefine $E = \exp(\mathrm{i}\alpha y) \to \exp[\mathrm{i}\alpha(y - c_{11}\,t_0)]$, where $c_{11} = -\sigma^I/\alpha$ is the wave speed according to linear theory, and consequently we then have that $\tilde{A} \to A$.

6. Mean flow correction and second harmonic

(i) Second-order non-periodic terms ($\varepsilon^2 E^0$) contribute to the equations for the mean flow. They can be written in operator form

$$\mathbf{L}_{0,2\sigma^R}\boldsymbol{w}_{20} = \boldsymbol{f}_{20}, \tag{29}$$

where $\boldsymbol{w}_{20} = (u_{20}, v_{20}, T_{20}, \Pi_{20})^T$ satisfies the total mass conservation and zero mass flux conditions

$$\left.\begin{aligned} \int_0^1 \rho_{20}\,\mathrm{d}x = 0, \\ \int_0^1 (\rho_{20} v_{00} + \rho_{00} v_{20} + 2\,\mathrm{Re}\{\rho_{11} v^*_{11}\})\,\mathrm{d}x = 0, \end{aligned}\right\} \tag{30}$$

and boundary conditions $u_{20} = v_{20} = T_{20} = 0$ at $x = 0$ and $x = 1$. As in §4, it can be shown that $\Pi_{20}(x; y) = \Pi'_{20}(x) + \bar{\Pi}_{20} y$, where $\bar{\Pi}_{20}$ is the value of the spatially uniform vertical dynamic pressure gradient induced by the disturbance. In the above equation, we denote the real part of the expression by $\mathrm{Re}\{\cdot\}$, and we note that at this order the equations are real since the imaginary part cancels identically. The expressions for $\boldsymbol{f}_{20} = (f_{20}^{(1)}, f_{20}^{(2)}, f_{20}^{(3)}, f_{20}^{(4)})^T$ are not given here since they are quite lengthy, but can be found in Suslov (1997). If at least one of the eigenvalues of problem (27), say σ_0, corresponding to $\alpha = 0$ is real for some set of parameters (ϵ, Gr) and

$$2\sigma^R(\alpha) = \sigma_0 \tag{31}$$

for some finite value of α and the same set of parameters (ϵ, Gr), then system (29) is not solvable and expansions (13)–(17) and (18) are not uniformly valid unless the orthogonality condition $\langle \boldsymbol{w}_{10}^\dagger, \boldsymbol{f}_{20} \rangle = 0$ is satisfied, where $\boldsymbol{w}_{10}^\dagger$ is the solution of the adjoint eigenvalue problem $\mathbf{L}_{0,\sigma_0}^\dagger \boldsymbol{w}_{10}^\dagger = 0$ with corresponding boundary conditions, and

$$\langle \boldsymbol{w}, \boldsymbol{f} \rangle = \int_0^1 (\boldsymbol{w} \cdot \boldsymbol{f})\, \mathrm{d}x. \tag{32}$$

This corresponds to the resonant interaction between the $\alpha = 0$ disturbance $\boldsymbol{w}_{10}$ (not necessarily the most unstable one), and the mean flow. In order to resolve this issue one would have to assume that $\boldsymbol{w}_{10} \neq 0$ from the very beginning (see that Lemma in Appendix A) and include corresponding terms in the resulting expansions, but this is beyond the scope of the present investigation. Subsequently, while we identify parameter values (ϵ, Gr) for which (31) is satisfied, we will only discuss results for parameter values for which (31) does not hold.

(ii) Collecting terms of order $\varepsilon^2 E^1$, we simply get

$$\frac{\partial A}{\partial t_1} \boldsymbol{B} \boldsymbol{w}_{11} = 0 \quad \text{or} \quad \frac{\partial A}{\partial t_1} = 0, \tag{33}$$

since $\boldsymbol{B}\boldsymbol{w}_{11} \not\equiv 0$. Thus disturbances do not evolve with respect to the slow time t_1, so

$$A(t) = A(t_0, t_2, \ldots). \tag{34}$$

Note that in the resonant case discussed above (when $\boldsymbol{w}_{10} \neq 0$) equations (33) are not homogeneous and the disturbance amplitude will then depend on the slow time t_1.

(iii) Collecting $\varepsilon^2 E^2$ terms we obtain

$$\mathbf{L}_{2\alpha, 2\sigma} \boldsymbol{w}_{22} = \boldsymbol{f}_{22}, \tag{35}$$

where $\boldsymbol{w}_{22} = (u_{22}, v_{22}, T_{22}, \Pi_{22})^T$, $u_{22} = v_{22} = T_{22} = 0$ at $x = 0$ and $x = 1$ and the components of $\boldsymbol{f}_{22} = (f_{22}^{(1)}, f_{22}^{(2)}, f_{22}^{(3)}, f_{22}^{(4)})^T$ are given in Suslov (1997). The total mass conservation and zero mass flux conditions are satisfied automatically because of the periodicity of the second harmonic.

Equation (35) reveals another unsolvable case: the 1:2 resonance between the fundamental and second-harmonic modes. The resonance will arise if for some fixed pair of parameters (ϵ, Gr), 2σ is one of the eigenvalues of problem (27) corresponding to wavenumber 2α. This resonance can be dealt with if we allow $\boldsymbol{w}_{12} \neq 0$ (see the Lemma in Appendix A). This also will lead to the dependence of the amplitude on the slow time t_1. Summarizing, we state both resonance conditions as

$$\sigma_i^I(0) = 0, \quad \sigma_i^R(0) = 2\sigma_j^R(\alpha) \tag{36}$$

and

$$\sigma_i(2\alpha) = 2\sigma_j(\alpha) \tag{37}$$

for some i and j and fixed parameters (ϵ, Gr). Both conditions can be easily satisfied in the Boussinesq limit since then, according to linear theory, the most unstable disturbances are found to be stationary, i.e. the eigenvalues σ_i are real. The 1:2 resonant interactions in the Boussinesq case were investigated in Fujimura & Mizushima (1987) and Fujimura 1992(*b*). Analysis of the resulting coupled amplitude equations predicts the dominating character of shorter-wavelength disturbances and the resonant decay of longer-wavelength disturbances even in linearly unstable regions. These results are consistent with computational results obtained using a Fourier–Chebyshev collocation technique reported in Mizushima & Saito (1987) and Mizushima (1990). The possibility of the above resonances in the non-Boussinesq case is discussed in later sections.

7. Landau equation

As shown above, when the disturbance amplitude is very small, it grows exponentially in the linearly unstable regions. In order to examine the possible saturation of the amplitude, we proceed to look at the equations that arise at order $\varepsilon^3 E^1$:

$$A|A|^2(\mathbf{L}_{\alpha,\sigma} - 2\sigma^R \boldsymbol{B})\, \boldsymbol{w}_{31} = \frac{\partial A}{\partial t_2} \boldsymbol{B} \boldsymbol{w}_{11} + A\,|A|^2 \boldsymbol{f}_{31}, \tag{38}$$

where $\boldsymbol{w}_{31} = (u_{31}, v_{31}, T_{31}, \Pi_{31})^T$, $u_{31} = v_{31} = T_{31} = 0$ and $x = 0$ and $x = 1$ and the components of the vector $\boldsymbol{f}_{31} = (f_{31}^{(1)}, f_{31}^{(2)}, f_{31}^{(3)}, f_{31}^{(4)})^T$ are given in Suslov (1997).

The linear system (38) is unconditionally solvable if $\sigma + 2\sigma^R$ is not an eigenvalue of problem (27). This is typically true when the parameters (ϵ, Gr) are chosen so as not to fall on the marginal stability surface (i.e. $\sigma^R \neq 0$). Since no solvability condition is necessary in this case to find a solution of (38), the definition of the Landau constant relating the disturbance amplitude and its slow time derivative requires some other condition. In the context of the amplitude expansion approach, this issue was first addressed by Herbert (1983) and later discussed by Fujimura (1988). Herbert proposed fixing the disturbance at some arbitrarily chosen location x_0 so as to be completely defined by the product $A\boldsymbol{w}_{11}(x_0)$. Subsequently, all other terms in the expansion vanish at this point. As shown in Appendix C, this procedure is inherently inconsistent. For this reason here we propose a different approach. Using the linearity of the problem, when $\sigma^R \neq 0$, we look for the solution in the form

$$\boldsymbol{w}_{31} = \boldsymbol{\chi}_1 + \boldsymbol{\chi}_2, \tag{39}$$

where $\boldsymbol{\chi}_{1,2} = (u_{\chi 1,2}, v_{\chi 1,2}, T_{\chi 1,2}, \Pi_{\chi 1,2})^T$ are solutions of the following problems:

$$(\mathbf{L}_{\alpha,\sigma} - 2\sigma^R \boldsymbol{B})\, \boldsymbol{\chi}_1 = \boldsymbol{f}_{31}, \tag{40}$$

and

$$A|A|^2(\mathbf{L}_{\alpha,\sigma} - 2\sigma^R \boldsymbol{B})\, \boldsymbol{\chi}_2 = \frac{\partial A}{\partial t_2} \boldsymbol{B} \boldsymbol{w}_{11}, \tag{41}$$

with $u_{\chi 1,2} = v_{\chi 1,2} = T_{\chi 1,2} = 0$ at $x = 0$ and $x = 1$. System (40) is solvable for any right-hand side. In addition, using separation of variables, one can see that system (41) is solvable only if

$$\partial A / \partial t_2 = KA\,|A|^2, \tag{42}$$

where $K = K^R + \mathrm{i}K^I$ is the complex separation constant (usually referred to as the first Landau constant). Then, using (27), we see that system (41) has the unique solution

$$\boldsymbol{\chi}_2 = -\frac{K}{2\sigma^R}\boldsymbol{w}_{11}. \tag{43}$$

Next, we project the solution of (40) on the $\boldsymbol{w}_{11}$-direction and write it as

$$\boldsymbol{\chi}_1 = r\boldsymbol{w}_{11} + \hat{\boldsymbol{\chi}}_1, \tag{44}$$

where

$$r = \frac{\langle \boldsymbol{w}_{11}, \boldsymbol{\chi}_1 \rangle}{\langle \boldsymbol{w}_{11}, \boldsymbol{w}_{11} \rangle} \quad \text{and} \quad \hat{\boldsymbol{\chi}}_1 \perp \boldsymbol{w}_{11}. \tag{45}$$

Combining terms in (13)–(17) corresponding to mode E^1 we obtain

$$\varepsilon A\{[1 + \varepsilon^2 |A^2| (r - K/2\sigma^R)]\, \boldsymbol{w}_{11} + \varepsilon^2 |A|^2 \hat{\boldsymbol{\chi}}_1 + \ldots\} E^1. \tag{46}$$

In order to remove the redundancy in the ε^3 terms, we should choose

$$K = 2\sigma^R r. \tag{47}$$

Note that any other choice of the Landau constant destroys the uniform validity of the expansion (A 12) in the limit $\sigma^R \to 0$. Furthermore, we will now show that definition (47) of the Landau constant in the limit $\sigma^R \to 0$ is identical to the one obtained from the conventional solvability condition, i.e. we show that

$$\lim_{\sigma^R \to 0} K = -\langle \boldsymbol{w}_{11}^\dagger, \boldsymbol{f}_{31} \rangle, \tag{48}$$

where $\boldsymbol{w}_{11}^\dagger$ is the solution of the problem adjoint to (27) and defined as

$$\mathbf{L}_{\alpha,\sigma}^\dagger \boldsymbol{w}_{11}^\dagger = 0 \tag{49}$$

with corresponding boundary conditions. Considering the inner product of $\boldsymbol{w}_{11}^\dagger$ with (38), taking into account the normalization for the adjoint eigenvector

$$\langle \boldsymbol{w}_{11}^\dagger, \boldsymbol{B}\boldsymbol{w}_{11} \rangle = 1 \tag{50}$$

and condition (42), and using (49), we obtain

$$-2\sigma^R \langle \boldsymbol{w}_{11}^\dagger, \boldsymbol{B}\boldsymbol{w}_{31} \rangle = K + \langle \boldsymbol{w}_{11}^\dagger, \boldsymbol{f}_{31} \rangle, \tag{51}$$

or, using (39), (43), (44), and (47),

$$K = -\langle \boldsymbol{w}_{11}^\dagger, \boldsymbol{f}_{31} \rangle - 2\sigma^R \langle \boldsymbol{w}_{11}^\dagger, \boldsymbol{B}\hat{\boldsymbol{\chi}}_1 \rangle. \tag{52}$$

The character of the singularity in (46) when $\sigma^R \to 0$ suggests that the function $\boldsymbol{\chi}_1$ can be decomposed as

$$\boldsymbol{\chi}_1 = \frac{1}{\sigma^R}\boldsymbol{\chi}_1^0 + \boldsymbol{\chi}_1^1, \tag{53}$$

where $\boldsymbol{\chi}_1^0$ and $\boldsymbol{\chi}_1^1$ are bounded and non-zero as $\sigma^R \to 0$. Substituting (53) into (40) we obtain

$$\frac{1}{\sigma^R}\mathbf{L}_{\alpha,\sigma}\boldsymbol{\chi}_1^0 - 2\boldsymbol{B}\boldsymbol{\chi}_1^0 + \mathbf{L}_{\alpha,\sigma}\boldsymbol{\chi}_1^1 - 2\sigma^R \boldsymbol{B}\boldsymbol{\chi}_1^1 = \boldsymbol{f}_{31}. \tag{54}$$

Taking the limit $\sigma^R \to 0$ we conclude that the condition

$$\lim_{\sigma^R \to 0} \frac{1}{\sigma^R}\mathbf{L}_{\alpha,\sigma}\boldsymbol{\chi}_1^0 < \infty \tag{55}$$

is necessary for (54) to be solvable. This is possible only if

$$\lim_{\sigma^R \to 0} \mathbf{L}_{\alpha,\sigma} \boldsymbol{\chi}_1^0 = 0 \tag{56}$$

and then $\boldsymbol{\chi}_1^0$ is non-trivial if and only if

$$\lim_{\sigma^R \to 0} \boldsymbol{\chi}_1^0 = r_1 \boldsymbol{w}_{11}, \tag{57}$$

where r_1 is some non-zero constant. Then term-by-term comparison of (44) and (53) gives that $\tilde{\boldsymbol{\chi}}_1 \sim \boldsymbol{\chi}_1^1$ and, consequently, is bounded, and $r = O(1/\sigma^R)$ as $\sigma^R \to 0$, so that finally from (52) we easily obtain (48). Note that although the Landau constant defined through Herbert's (1983) approach as $\sigma^R \to 0$ tends to the same limit (48), in general it differs from the one defined above for any finite value of σ^R.

In contrast to Herbert's approach, for the chosen normalization (28) the above procedure results in a unique definition of the Landau constant on the marginal stability surface as well as away from it since the projection r is defined uniquely. In other words, in the present approach we have eliminated the source of inconsistency arising in Herbert's approach from the attempt to define a global quantity such as the Landau constant using some local property of the spatial solution (i.e. the value at an arbitrarily chosen point). The present approach also completely removes the redundancy in expansion (46), guarantees its uniformity for small amplitudes in the resonance-free regions of the parameter space, and shows that the fundamental disturbance mode $\boldsymbol{w}_{11}$ necessarily induces its own orthogonal distortion ($\tilde{\boldsymbol{\chi}}_1$) at higher orders of ε which cannot be removed by the normalization of the disturbance amplitude as assumed by Herbert.

Reconstituting the time derivative of the amplitude, we now have

$$\frac{\mathrm{d}A}{\mathrm{d}t} = \frac{\partial A}{\partial t_0} + \varepsilon^2 \frac{\partial A}{\partial t_2} + \ldots = \sigma^R A + \varepsilon^2 K A |A|^2 + \ldots. \tag{58}$$

Noting that ε is just a formal expansion parameter used to distinguish different orders in amplitude, we redefine $\varepsilon A \to A$, and neglecting higher orders of amplitude we obtain the Landau equation

$$\mathrm{d}A/\mathrm{d}t = \sigma^R A + K A |A|^2. \tag{59}$$

Since we can write $A = |A| \mathrm{e}^{\mathrm{i}\theta}$, then this equation is equivalent to two equations for the modulus and phase:

$$\mathrm{d}|A|/\mathrm{d}t = \sigma^R |A| + K^R |A|^3, \tag{60}$$

$$\mathrm{d}\theta/\mathrm{d}t = K^I |A|^2. \tag{61}$$

Equation (60) can have two equilibrium solutions. The first, $|A_e| = 0$, always exists, but is stable only if $\sigma^R < 0$. The second equilibrium solution

$$|A_e| = (-\sigma^R/K^R)^{1/2} \tag{62}$$

only exists if $\sigma^R/K^R < 0$, and is stable if $\sigma^R > 0$. If this last equilibrium solution exists for $\sigma^R < 0$ ($K^R > 0$), i.e. before linear instability occurs, the bifurcation is subcritical, otherwise it is supercritical. Note that the cubic Landau equation (60) does not provide any stable finite-amplitude equilibrium for a subcritical bifurcation. In order to obtain a stable equilibrium solution in such case, it is necessary to carry the analysis to higher orders in amplitude. This will not be done in this work.

8. Two-mode interactions

The above analysis is not adequate in the vicinity of the codimension-2 point $(\epsilon_*, Gr_c(\epsilon_*))$ where shear and buoyant disturbance modes interact with each other (Suslov & Paolucci 1995*b*). In this situation the truncated amplitude expansions (13)–(17), again up to third order in amplitude, are generalized to

$$\begin{aligned} w(x,y,t) &= w_{000}(x)+|A_1(t)|^2 w^{(1)}_{200}(x)+|A_2(t)|^2 w^{(2)}_{200}(x) \\ &\quad +\{[A_1(t)\,(w_{110}(x)+|A_1(t)|^2 w^{(1)}_{310}(x)+|A_2(t)|^2 w^{(2)}_{310}(x))\,E_1+A_1^2(t)\,w_{220}(x)\,E_1^2 \\ &\quad +[A_2(t)\,(w_{101}(x)+|A_1(t)|^2 w^{(1)}_{301}(x)+|A_2(t)|^2 w^{(2)}_{301}(x))\,E_2+A_2^2(t)\,w_{202}(x)\,E_2^2 \\ &\quad +A_1(t)\,A_2^*(t)\,w_{21-1}(x)\,E_1\,E_2^*+A_1(t)\,A_2(t)\,w_{211}(x)\,E_1\,E_2]+\text{c.c.}\}, \end{aligned} \tag{63}$$

$$\begin{aligned} \Pi(x,y,t) &= \bar{\Pi}_{000}\,y+|A_1(t)|^2(\Pi^{(1)}_{200}(x)+\bar{\Pi}^{(1)}_{200}y)+|A_2(t)|^2(\Pi^{(2)}_{200}(x)+\bar{\Pi}^{(2)}_{200}y) \\ &\quad +\{[A_2(t)\,(\Pi_{101}(x)+|A_1(t)|^2\Pi^{(1)}_{301}(x)+|A_2(t)|^2\Pi^{(2)}_{301}(x))\,E_2+A_2^2(t)\,\Pi_{202}(x)\,E_2^2 \\ &\quad +[A_1(t)\,(\Pi_{110}(x)+|A_1(t)|^2\Pi^{(1)}_{310}(x)+|A_2(t)|^2\Pi^{(2)}_{310}(x))\,E_1+A_1^2(t)\,\Pi_{220}(x)\,E_1^2 \\ &\quad +A_1(t)\,A_2^*(t)\,\Pi_{21-1}(x)\,E_1\,E_2^*+A_1(t)\,A_2(t)\,\Pi_{211}(x)\,E_1\,E_2]+\text{c.c.}\}, \end{aligned} \tag{64}$$

$$P(t) = P_{000}+|A_1(t)|^2 P^{(1)}_{200}+|A_2(t)|^2 P^{(2)}_{200}, \tag{65}$$

where w represents u, v, or T, the first index corresponds to the order of the amplitude, and the second and third indices to powers of $E_1 = \exp[\mathrm{i}\alpha_1(y-c_{110}\,t_0)]$ and $E_2 = \exp[\mathrm{i}\alpha_2(y-c_{101}\,t_0)]$, respectively. Wave speeds, according to linear theory, are defined as $c_{110} = -\sigma_1^I/\alpha_1$ and $c_{101} = -\sigma_2^I/\alpha_2$. Superscripts (1) and (2) are used to indicate the terms associated with the mean flow correction corresponding to the shear and buoyant modes respectively. The two-mode interactions do not add additional terms to the expansion (65) for the thermodynamic pressure. These expansions are complete up to the third order in amplitude for Fourier modes E_1 and E_2 provided that no wavenumber resonance is present at least up to third order, i.e.

$$\alpha_1 \neq n\alpha_2, \quad n = 1, 2, 3. \tag{66}$$

The property vector $\boldsymbol{g} = (\rho, c_p, \mu, k)^T$ is expanded similarly:

$$\left.\begin{aligned} \boldsymbol{g}_{110} &= \boldsymbol{g}_{000T}\,T_{110}, \\ \boldsymbol{g}^{(1)}_{200} &= \boldsymbol{g}_{000T}\,T^{(1)}_{200}+\boldsymbol{g}_{000TT}\,|T_{110}|^2+\boldsymbol{g}_{000P}\,P^{(1)}_{200}, \\ \boldsymbol{g}_{220} &= \boldsymbol{g}_{000T}\,T_{220}+\tfrac{1}{2}\boldsymbol{g}_{000TT}\,T^2_{110}, \\ \boldsymbol{g}^{(1)}_{310} &= \boldsymbol{g}_{000T}\,T^{(1)}_{310}+\boldsymbol{g}_{000TT}(T_{110}\,T^{(1)}_{200}+T^*_{110}\,\mathrm{T}_{220})+\tfrac{1}{2}\boldsymbol{g}_{000TTT}\,T_{110}\,|T_{110}|^2 \\ &\quad +\boldsymbol{g}_{000TP}\,T_{110}\,P^{(1)}_{200}, \\ \boldsymbol{g}_{101} &= \boldsymbol{g}_{000T}\,T_{101}, \\ \boldsymbol{g}^{(2)}_{200} &= \boldsymbol{g}_{000T}\,T^{(2)}_{200}+\boldsymbol{g}_{000TT}\,|T_{101}|^2+\boldsymbol{g}_{000P}\,P^{(2)}_{200}, \\ \boldsymbol{g}_{202} &= \boldsymbol{g}_{000T}\,T_{202}+\tfrac{1}{2}\boldsymbol{g}_{000TT}\,T^2_{101}, \\ \boldsymbol{g}^{(2)}_{301} &= \boldsymbol{g}_{000T}\,T^{(2)}_{310}+\boldsymbol{g}_{000TT}(T_{101}\,T^{(2)}_{200}+T^*_{101}\,T_{202}) \\ &\quad +\tfrac{1}{2}\boldsymbol{g}_{000TTT}\,T_{101}\,|T_{101}|^2+\boldsymbol{g}_{000TP}\,T_{101}\,P^{(2)}_{200}, \\ \boldsymbol{g}_{21-1} &= \boldsymbol{g}_{000T}\,T_{21-1}+\boldsymbol{g}_{000TT}T_{110}\,T^*_{101}, \\ \boldsymbol{g}_{211} &= \boldsymbol{g}_{000T}\,T_{211}+\boldsymbol{g}_{000TT}\,T_{110}\,T_{101}, \\ \boldsymbol{g}^{(2)}_{310} &= \boldsymbol{g}_{000T}\,T^{(2)}_{310}+\boldsymbol{g}_{000TT}(T_{110}\,T^{(2)}_{200}+T_{101}\,T_{21-1}+T^*_{101}\,T_{211})+\boldsymbol{g}_{000TTT}\,T_{110}\,|T_{101}|^2 \\ &\quad +\boldsymbol{g}_{000TP}\,T_{110}\,P^{(2)}_{200}, \\ \boldsymbol{g}^{(1)}_{301} &= \boldsymbol{g}_{000T}\,T^{(1)}_{301}+\boldsymbol{g}_{000TT}(T_{101}\,T^{(1)}_{200}+T_{110}\,T^*_{21-1}+T^*_{110}\,T_{211})+\boldsymbol{g}_{000TTT}\,T_{101}\,|T_{110}|^2 \\ &\quad +\boldsymbol{g}_{000TP}\,T_{101}\,P^{(1)}_{200}. \end{aligned}\right\} \tag{67}$$

Equations for each separate mode up to second order in amplitude were considered in the previous sections. The equations at second order in amplitude responsible for mode coupling can be written as

$$\mathbf{L}_{\alpha_1-\alpha_2,\sigma_1-\sigma_2}\,\boldsymbol{w}_{21-1}=\boldsymbol{f}_{21-1},\quad \mathbf{L}_{\alpha_1+\alpha_2,\sigma_1+\sigma_2}\,\boldsymbol{w}_{211}=\boldsymbol{f}_{211}, \tag{68}$$

where $\boldsymbol{w}_{21-1}=(u_{21-1},v_{21-1},T_{21-1},\Pi_{21-1})^T$, $\boldsymbol{w}_{211}=(u_{211},v_{211},T_{211},\Pi_{211})^T$, $u_{21-1}=v_{21-1}=T_{21-1}=u_{211}=v_{211}=T_{211}=0$ at $x=0$ and $x=1$ and the components of $\boldsymbol{f}_{21-1}=(f^{(1)}_{21-1}, f^{(2)}_{21-2}, f^{(3)}_{21-1}, f^{(4)}_{21-1})^T$ and $\boldsymbol{f}_{211}=(f^{(1)}_{211}, f^{(2)}_{211}, f^{(3)}_{211}, f^{(4)}_{211})^T$ are given in Suslov (1997).

At third order in amplitude, for the Fourier mode E_1 we now obtain the system of equations

$$A_1|A_1|^2(\mathbf{L}_{\alpha_1,\sigma_1}-2\sigma_1^R\boldsymbol{B})\,\boldsymbol{w}^{(1)}_{310}+A_1|A_2|^2(\mathbf{L}_{\alpha_1,\sigma_1}-2\sigma_2^R\boldsymbol{B})\,\boldsymbol{w}^{(2)}_{310}$$
$$=\frac{\partial A_1}{\partial t_2}\boldsymbol{B}\boldsymbol{w}_{110}+A_1(|A_1|^2\boldsymbol{f}^{(1)}_{310}+|A_2|^2\boldsymbol{f}^{(2)}_{310}), \tag{69}$$

where $\boldsymbol{f}^{(1)}_{310}$ (previously named $\boldsymbol{f}_{31}$) and $\boldsymbol{f}^{(2)}_{310}$ are given in Suslov (1997). A similar system is obtained for the Fourier mode E_2. Then application of the theory derived earlier and reconstitution of the full time derivative lead to the coupled Landau equations

$$\frac{\mathrm{d}A_i}{\mathrm{d}t}=\sigma_i^R A_1+\sum_{j=1}^{2}K_{ij}A_i|A_j|^2,\quad i=1,2. \tag{70}$$

The Landau constants are defined as

$$K_{ij}=2\sigma_j^R\frac{\langle \boldsymbol{w}_{1\delta_{i,1}\delta_{i,2}},\boldsymbol{\chi}_{1ij}\rangle}{\langle \boldsymbol{w}_{1\delta_{i,1}\delta_{i,2}},\boldsymbol{w}_{1\delta_{i,1}\delta_{i,2}}\rangle}, \tag{71}$$

where $\delta_{i,j}$ is the Kronecker symbol and $\boldsymbol{\chi}_{1ij}$ are solutions of the associated problems

$$(\mathbf{L}_{\alpha_i,\sigma_i}-2\sigma_j^R\boldsymbol{B})\,\boldsymbol{\chi}_{1ij}=\boldsymbol{f}^{(j)}_{3\delta_{i,1}\delta_{i,2}},\quad i,j=1,2. \tag{72}$$

By introducing polar notation $A_j=|A_j|\,\mathrm{e}^{\mathrm{i}\theta_j}$, $j=1,2$, the coupled Landau equations are rewritten as

$$\mathrm{d}|A_j|/\mathrm{d}t=|A_j|(\sigma_j^R+K^R_{j1}|A_1|^2+K^R_{j2}|A_2|^2), \tag{73}$$
$$\mathrm{d}\theta_j/\mathrm{d}t=K^I_{j1}|A_1|^2+K^I_{j2}|A_2|^2. \tag{74}$$

We distinguish four equilibrium solutions of equation (73):

$$\left.\begin{array}{ll}
\text{(i)} & |A_{1e}|=|A_{2e}|=0,\\
\text{(ii)} & |A_{2e}|=0,\quad |A_{1e}|^2=-\sigma_1^R/K^R_{11}>0,\\
\text{(iii)} & |A_{1e}|=0,\quad |A_{2e}|^2=-\sigma_2^R/K^R_{22}>0,\\
\text{(iv)} & |A_{1e}|^2=\dfrac{\sigma_2^R K^R_{12}-\sigma_1^R K^R_{22}}{K^R_{11}K^R_{22}-K^R_{12}K^R_{21}}>0,\quad |A_{2e}|^2=\dfrac{\sigma_1^R K^R_{21}-\sigma_2^R K^R_{11}}{K^R_{11}K^R_{22}-K^R_{12}K^R_{21}}>0.
\end{array}\right\} \tag{75}$$

The first solution corresponds to the linearly stable case when $\sigma_1^R<0$ and $\sigma_2^R<0$. The second and third solutions have been analysed before in the context of the one-mode analysis. The last solution results from the two-mode interactions. In order to investigate the stability of the solutions we linearize (73) about an equilibrium solution and find the eigenvalues of the resulting system to be

$$\lambda_{1,2}=\frac{C_{11}+C_{22}}{2}\left[1\pm\left(1+16\frac{|A_{1e}|^2|A_{2e}|^2K^R_{12}K^R_{21}}{(C_{11}+C_{22})^2}\right)^{1/2}\right], \tag{76}$$

where

$$\left.\begin{aligned} C_{11} &= \sigma_1^R + 3\,|A_{1e}|^2\,K_{11}^R + |A_{2e}|^2\,K_{12}^R, \\ C_{22} &= \sigma_2^R + 3\,|A_{2e}|^2\,K_{22}^R + |A_{1e}|^2\,K_{21}^R. \end{aligned}\right\} \tag{77}$$

We now observe that the finite-amplitude equilibria are stable only if $K_{12}^R K_{21}^R < 0$ and $C_{11} + C_{22} < 0$.

Introducing

$$r_1 = |A_2| K_{22}^R|^{1/2}, \quad r_2 = |A_1| K_{11}^R|^{1/2}, \quad \mu_1 = -\sigma_2^R, \quad \mu_2 = -\sigma_1^R, \tag{78}$$

$$\left.\begin{aligned} b &= -K_{21}^R/|K_{11}^R|, \\ c &= -K_{12}^R/|K_{22}^R|, \end{aligned}\right\} \quad d = \begin{cases} 1 & \text{if} \quad K_{11}^R < 0 \\ -1 & \text{if} \quad K_{11}^R > 0, \end{cases} \tag{79}$$

and inverting time $t \to -t$ we can rewrite system (73) as

$$\dot{r}_1 = r_1(\mu_1 + r_1^2 + b r_2^2), \quad \dot{r}_2 = r_2(\mu_2 + c r_1^2 + d r_2^2), \tag{80}$$

which was analysed in detail by Guckenheimer & Holmes (1983). Here we took into account that, as discussed in the next Section, $K_{22}^R < 0$ for all values of governing parameters considered. Note that although it is possible to classify the fixed points by considering only equation (80), in order to interpret the complete flow dynamics one should consider the four-dimensional system which includes the disturbance phases.

9. Results

All numerical results are obtained using a Chebyshev pseudo-spectral approximation in the horizontal direction (Suslov & Paolucci 1995*a*, *b*). The number of modes used in all cases is 48, which convergence tests have shown to guarantee the accuracy of all results to within 1 %. The resulting algebraic problems are solved in double precision using the following routines from the IMSL mathematical library (IMSL 1989): NEQNF to solve the basic flow problem (22), GVCCG and GVLRG to solve the generalized eigenvalue problem (27) for $\alpha > 0$ and $\alpha = 0$ respectively, LSBRR to solve for the mean flow correction (equations (29)–(30)), and LSACG to solve for the second harmonic and for χ_1 ((35) and (40) respectively). Furthermore, the coupled Landau equations (70) are integrated in time using a Gear algorithm as implemented in routine IVPAG. We also note that in reporting all numerical results in the Boussinesq limit of $\epsilon \ll 1$ (corresponding to the mathematical limit $\epsilon \to 0$) we actually use the value of $\epsilon = 5 \times 10^{-3}$ for computations.

9.1. *Validity of Landau equations*

Equation (59) has been derived using two explicit assumptions: the disturbance amplitude is small and there exist multiple timescales in the problem. These conditions do not impose any direct limitation on the region of applicability in parameter space, but restrict the initial disturbance to consist of only a small-amplitude mode corresponding to a chosen wavenumber α (in other words, it is assumed that an arbitrary initial disturbance asymptotically approaches the mode with wavenumber α). The choice of the fast timescale t_0 is associated with the exponential development of the disturbance while it is small. After the disturbance reaches the finite amplitude such that the nonlinear terms become important, the temporal behaviour of the disturbances deviates from exponential ('slows down'). This is characterized by different long timescales. Thus the fact that the exponential disturbance growth or decay always changes its character in the vicinity of equilibrium justifies the introduction of the proposed timescales which are functions of the amplitude size only but do not require

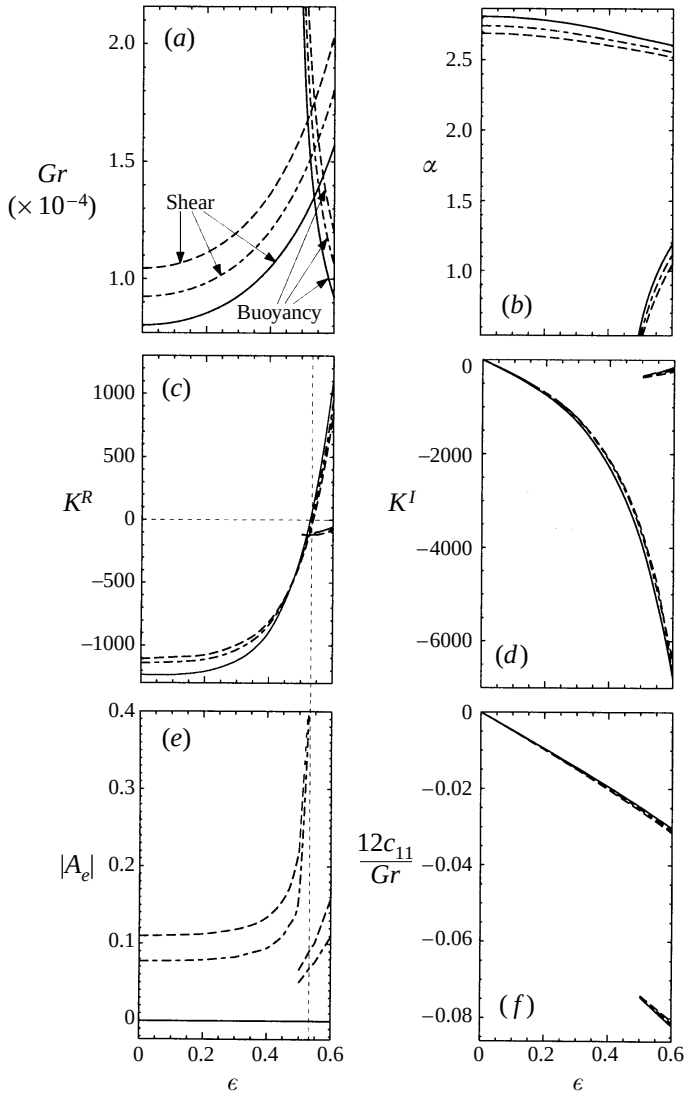

FIGURE 1. (*a*) Grashof number, (*b*) wavenumber, (*c*) real and (*d*) imaginary parts of the first Landau constant, and (*f*) wavespeed as functions of ϵ for $\delta = 0$ (solid lines), $\delta = 0.15$ (dash-dotted lines), and $\delta = 0.3$ (dashed lines).

the linear amplification/decay rate $|\sigma^R|$ to be essentially small. Then (59) describes the dynamics of the problem correctly as long as the disturbance amplitude remains small. A wavenumber selection mechanism is missing. However, it is generally assumed (but rarely discussed) that the wavenumber selected by the flow corresponds to the wavenumber having maximum amplification based on linear analysis. In most regions of parameter space considered in this work, the equilibrium amplitude resulting from (59) is sufficiently small to allow us to track the complete process of disturbance growth by keeping only terms up to third order in amplitude. In order to illustrate this, some nonlinear results are plotted in figure 1 as functions of ϵ. Results are given for values of $\delta \equiv (Gr - Gr_c)/Gr_c = 0$, 0.15, and 0.3, denoted by solid, dash-dotted, and dashed lines respectively. All lines corresponding to the buoyant instability are plotted only for

$0.45 \lesssim \epsilon \lesssim 0.6$ where buoyancy effects are significant. The wavenumbers corresponding to the largest linear growth rate in supercritical regimes are slightly lower than the respective ones on the critical curves and are presented in figure 1*b*).

Although the disturbance amplitude itself remains small, in general this is not sufficient for the amplitude expansion to be valid as discussed in Stuart (1960), Fujimura (1988), Benney & Bergeron (1969), Davis (1969), Benney & Maslow (1974) and Haberman (1972). It is shown that the uniformity of the expansion can be violated for a certain parameter range owing to the nearly singular behaviour of the linear eigenfunctions in critical layers. Such a situation typically arises in Poiseuille-type flows. As discussed in Suslov & Paolucci (1995*a*), the shear instability in natural convection flow in a vertical enclosure is associated with the inflection point, and the singularity in the Orr–Sommerfeld equation in this case is removable. Thus in this case the expansion is expected to remain uniform as long as $|A| \ll 1$. On the other hand, for the buoyant instability, the location of the critical layer does not coincide with the inflection point, and the restriction for the amplitude $\alpha Re|A|^{3/2} \ll 1$ given in Fujimura (1988) for Poiseuille-type flows can be estimated for the convection flow as $\sqrt{3}\alpha Gr|A|^{3/2}/216 \ll 1$. The numerical coefficient is based on the maximum value of the basic flow velocity (see Suslov & Paolucci 1995*a*). This solution is satisfied for all regimes discussed in the present paper.

Figures 1(*c*) and 1(*d*) show the behaviour of the first Landau constant K. Its real part is negative for $\epsilon < \epsilon_{**} \approx 0.528$. This means that the bifurcation is supercritical for Boussinesq and slightly non-Boussinesq flows. The value of K is real in the limit $\epsilon \to 0$ (see figure 1*d*). This is consistent with previously known Boussinesq results reported in Mizushima & Gotoh (1983) for $Pr = 7.5$ and in Fujimura & Mizushima (1987) for $Pr = 0$. At ϵ_{**} (vertical dotted line in figure 1*c*, *e*) the real part of the Landau constant corresponding to the shear-driven instability changes sign to positive, reflecting the fact that the bifurcation becomes subcritical for $\epsilon > \epsilon_{**}$. The equilibrium amplitude defined by (62) is plotted on figure 1(*e*). It remains small for $\epsilon \lesssim 0.45$, justifying the validity of the amplitude expansion (A 12). In the vicinity of ϵ_{**} the amplitude $|A_e|$ grows unboundedly according to (62). Thus, in order to obtain the saturation in the regions where the type of bifurcation changes, we must retain higher-order terms in formulae (13)–(18), and proceed to the higher-order Landau equation, but this is beyond the scope of our present work. The bifurcation associated with the buoyancy mode is always supercritical (the real part of the corresponding Landau constant is negative as shown on figure 1*c*). As a consequence, the equilibrium amplitude for the buoyant instability does not exhibit any singularity and remains sufficiently small for the present analysis to be valid.

As noted earlier, in deriving (59) we assumed that the initial disturbance could be represented by a single disturbance wave corresponding to an arbitrary wavenumber α which remains fixed as the instability develops. This assumption is valid in general only if the two leading eigenvalues $\sigma_1(\alpha)$ and $\sigma_2(\alpha)$ (which are not conjugate) are very well separated. This is found to be the case in the critical (see figure 2*a*, *e*) as well as in the sub- and supercritical regimes considered in the present work. Consideration of only one mode also poses an implicit limitation on the wavenumber range in which the analysis is valid. In order to illustrate this we refer to figure 2 where real and imaginary parts of the four leading eigenvalues and the first Landau constant associated with the most unstable disturbance mode are plotted as functions of the wavenumber for the shear-dominated instability in the Boussinesq limit (figure 2*a*—*d*) and for $\epsilon = 0.536$ (figure 2*e*–*h*), where the shear and buoyant modes compete with each other. The thick solid lines (which we shall call T for short) in figure 2(*a*, *b*, *e*, *f*) represent the eigenvalue

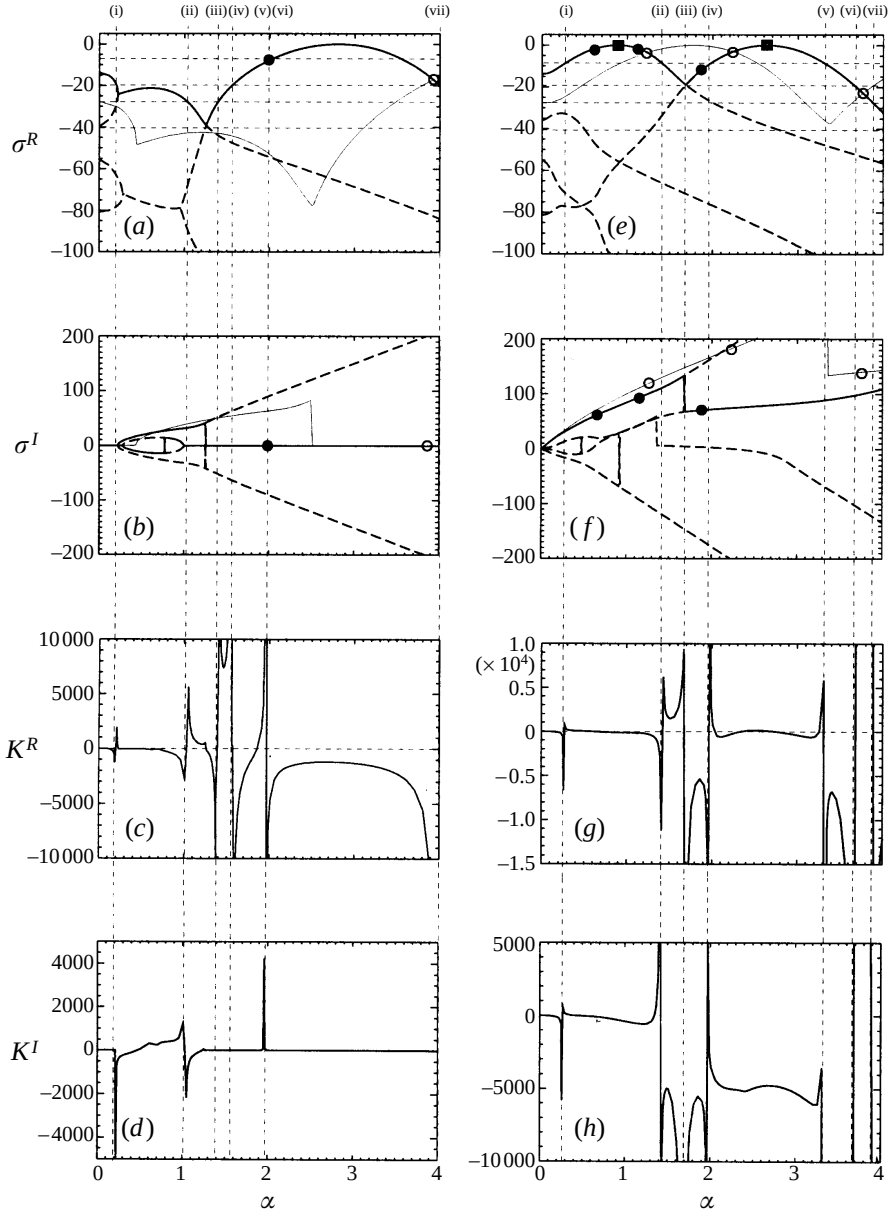

FIGURE 2. Leading eigenvalues and first Landau constant as functions of wavenumber for (*a–d*) $\epsilon \ll 1$, $Gr = Gr_c = 8037.6$ and (*e–h*) $\epsilon = 0.536$, $Gr = Gr_c = 13\,500$.

with the largest real part, $\sigma_1(\alpha)$. The other eigenvalues are plotted with dashed lines. In order to to give an easy geometrical interpretation of the resonance conditions (36) and (37), in figures 2(*a*) and 2(*e*) we show the curves $\sigma(\alpha) = 2\sigma_1(\alpha/2)$ as faint (F) lines and $\sigma^R(\alpha) = \frac{1}{2}\sigma_i^R(0)$, $i = 1, \ldots, 4$, as horizontal dotted (D) lines.

It can be easily seen that TF intersections (shown as open circles) and the respective points with one-half wavenumber (shown as filled circles on T) give us pairs of points where the 1:2 resonance between the fundamental disturbance mode (open circle) and its second harmonic (filled circle) could possibly exist. In fact, condition (37) is exactly satisfied in the Boussinesq limit for the pair of points denoted by circles in

figure 2(*a*, *b*). Owing to this resonance, the value of the first Landau constant becomes infinite at wavenumber labelled (v) in figure 2(*a–d*), which in turn leads to a vanishing equilibrium amplitude. Note that while lines (v) and (vi) (discussed below) appear to coincide in the figure, they are found to be numerically distinct. Although our analysis is incomplete in the vicinity of any resonant point, based on this result we can expect that the competition between the two resonating harmonics will lead to the fundamental mode decaying in favour of its second harmonic. This is exactly what is observed in Fujimura & Mizushima (1987) and Fujimura (1992*b*), where the resonant situation was analysed by deriving appropriate coupled amplitude equations.

In the non-Boussinesq regimes TF intersections and the respective points with one-half wavenumber in figure 2(*e*) do not correspond to resonant interactions since the instability is oscillatory in these cases (the disturbance wave speed $c_{11} = -\sigma^I/\alpha$ is negative and deviates substantially from zero as can be seen from figure 1*f*), and condition (37) is not satisfied for non-vanishing imaginary parts of the eigenvalues (none of the empty circles in figure 2*f* are TF intersections). Physically it means that although the real amplification growth rates for the two harmonics are in resonance, the phase speeds of the two waves are so different that the two harmonics do not interact with each other. Consequently, the two disturbance waves are completely decoupled from each other and the range of applicability of the one-mode analysis becomes larger in non-Boussinesq regimes.

The TD intersections correspond to resonances between the mean flow correction and disturbances with $\alpha = 0$ (see conditions (36)). The vertical line (vi) in figure 2(*a–d*) and lines (i), (ii), (iv), and (v) in figure 2(*e–h*) denote wavenumbers which correspond to resonant interactions with the most unstable eigenmode at $\alpha = 0$. Lines (i), (iv), and (vii) in Figure 2(*a–d*) and (iii) and (vi) in figure 2(*e–h*) denote wavenumbers that resonate with the second $\alpha = 0$ eigenmode. Lines (ii) and (iii) in figure 2(*a–d*) and (vii) in figure 2(*e–h*) denote wavenumbers that resonate with the third $\alpha = 0$ eigenmode. Again, the singularity of the first Landau constant suggests the decay of the resonating periodic disturbances in favour of the mean flow. We also note that this type of resonance is equally possible in both Boussinesq and non-Boussinesq regimes, since, as can be seen from figures 2(*b*) and 2(*f*), we have $\sigma_i^I(0) = 0$, $i = 1, 2, \ldots$. Although not shown here, this result remains true for all values of ϵ.

The linear investigation also showed that $\sigma_i^R(0) < 0$, $i = 1, 2, \ldots$, for all values of ϵ and Gr. This means that disturbances that decay according to linear theory can resonate with the $\alpha = 0$ modes. It can be easily shown by generalizing condition (31) that such resonances arise at the $2k$th order of ε in expansion (A 12), if

$$\sigma_i^R(0) = 2k\sigma_i^R(\alpha), \quad \sigma_i^I(0) = 0. \tag{81}$$

Since the number of eigenvalues with negative real parts is infinite, one can expect that for any α such that $\sigma_1^R(\alpha) < 0$ there always exists a pair $(i(\alpha), k(\alpha))$ for which (81) is satisfied (here i corresponds to the number of the eigenvalue in the ordered infinite sequence $0 > \sigma_1^R(0) > \ldots > \sigma_i^R(0) > \ldots$ and k is the order at which the resonance arises). Strictly speaking, this means that the infinite single-mode expansion (A 12) is not uniformly valid for subcritical flows (see similar discussions in Davey & Nguyen 1971 and Herbert 1983). In order to resolve this problem one would have to modify the expansion by adding the resonating modes (which depend on all timescales) starting at the ε^{2k-1}-order. It is important to note that the expansion for the lower orders in ε remains unchanged.

Summarizing, we conclude that the proposed weakly nonlinear analysis and derivation of the cubic Landau equation can be justified for a band of wavenumbers

centred at the critical value, within which no resonances are possible for disturbances up to cubic order in ε (for example, the wavenumber intervals between lines (vi) and (vii) on figure 2(*a–d*) and between lines (i) and (ii), and (iv) and (v) on figure 2(*e–h*). For α far from the critical value one should first examine the eigenvalues of the linearized problem at $\alpha = 0$ and 2α in order to find out whether a resonance is possible. If a resonance is present, a different form of the expansions is necessary as was noted earlier, although the overall procedure remains the same. In being aware of the possibility of different resonances, we did not find any 1:2 resonance in the non-Boussinesq regimes because of the oscillatory nature of the disturbances and stayed away from mean flow resonances at second order in ε (for numerical results in subcritical regimes which we present below we found $k > 10$ except at the points which have been discussed previously). Thus we conclude that the proposed theory can be successfully applied in a wide region of (ϵ, Gr, α) space as long as the amplitude remains sufficiently small.

We should remember that the single-mode analysis is also not adequate in the vicinity of the codimension-2 point $(\epsilon_*, Gr_c(\epsilon_*)) \approx (0.536, 13\,500)$ where two physically different modes, shown by squares in figure 2(*e*), can become unstable and compete with each other. Near this point, shown in more detail in figure 13, the disturbance amplitudes are properly described by the coupled Landau equations (70). Here, $\alpha_1 = 2.6370$ and $\alpha_2 = 0.8880$, and none of the conditions (66) are satisfied in the vicinity of $(\epsilon_*, Gr_c(\epsilon_*))$. Thus no wavenumber resonances are possible.

9.2. *Disturbed flow*

We first present the characteristics of the disturbed flow F averaged over the disturbance wavelength, where $F = F_{00} + |A|^2 F_{20}$, and F_{00} and F_{20} stand for basic flow and mean flow correction quantities respectively. While the value of the amplitude A depends strongly on the distance from the critical point, F_{20} changes slightly. For this reason it is convenient to present the quantities F_{20} evaluated at the critical points $(Gr_c(\epsilon), \alpha_c(\epsilon))$ (or along the solid curves in figure 1*a*, *b*) in examining the physical mechanisms of instability.

As we increase the temperature difference between the walls, the temperature and the density distributions in the enclosure deviate from the linear ones due to nonlinear property variations. As a consequence, in order to satisfy the mass conservation condition, the basic flow thermodynamic pressure decreases as shown in figure 3(*a*) (for a more extensive discussion of the basic flow see Chenoweth & Paolucci 1986 and Suslov & Paolucci 1995*a*). Analysis of shear- and buoyancy-driven instabilities shows that both disturbances lead to a further decrease in thermodynamic pressure (see figure 3*b*), thus amplifying the non-Boussinesq effects.

When the temperature difference between the walls is increased the local density in the vicinity of the hot wall becomes smaller because of two effects: a drop in the thermodynamic pressure and an increase in the local temperature. On the other hand, near the cold wall both the thermodynamic pressure and the local temperature decrease thus affecting the local density in opposite directions. Subsequently, the fluid in the cavity has the overall tendency to move up due to this buoyancy effect. However, the average mass flux must remain zero since the cavity is closed. This condition induces a positive vertical pressure gradient $\bar{\Pi}_{00}$, shown in figure 3(*c*), preventing a net upward flow. The form of the plot for $\bar{\Pi}_{00}$ resembles the critical curves $Gr(\epsilon)$ shown in figure 1(*a*) since the buoyancy forces to be opposed by the induced pressure gradient are proportional to the Grashof number. In addition, since the largest disturbances are located in the high-density region near the cold wall (see Suslov & Paolucci 1995*a*),

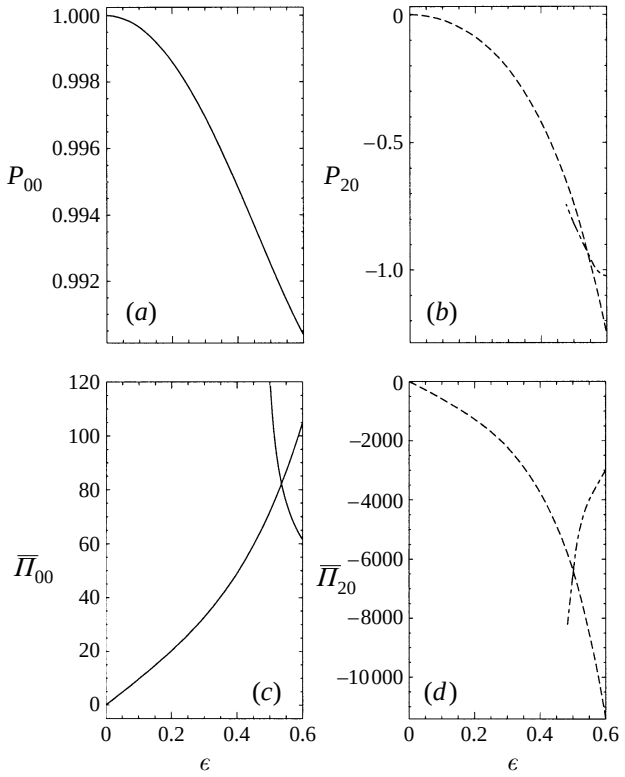

FIGURE 3. (*a*) and (*b*) Thermodynamic pressure and (*c*) and (*d*) dynamic pressure gradient for the basic flow and the mean flow correction as functions of ϵ. Dashed and dash-dotted lines correspond to shear and buoyant disturbances respectively.

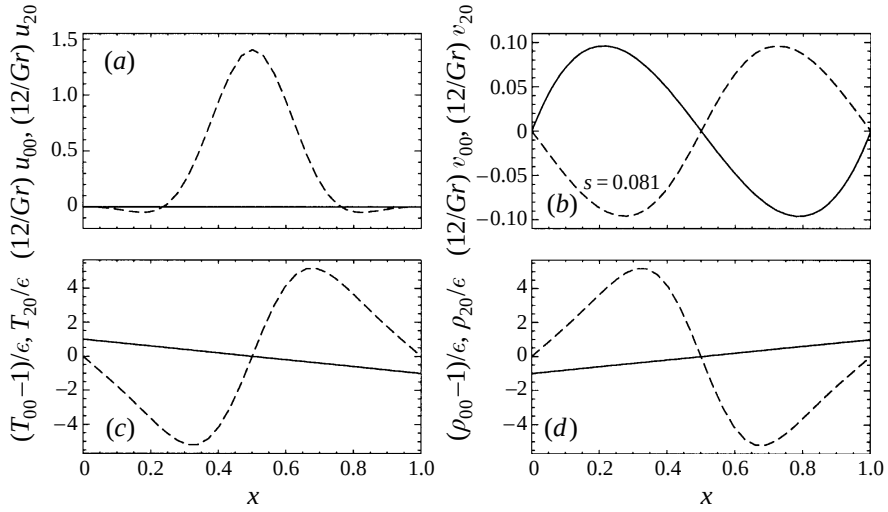

FIGURE 4. Basic flow (solid lines) and mean flow correction due to shear instability (dashed lines) for Gr_e in the Boussinesq limit $\epsilon \ll 1$. The scaling parameter s is introduced for plotting purposes.

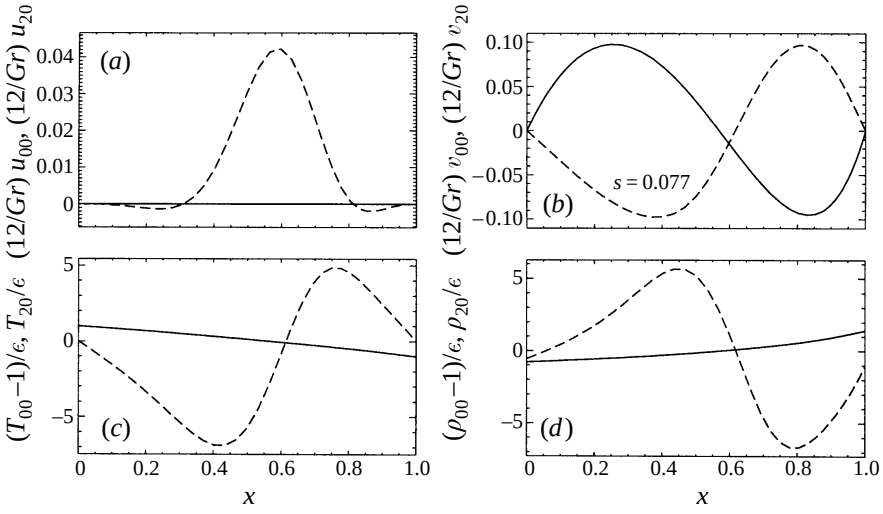

FIGURE 5. As figure 4 but for the non-Boussinesq case of $\epsilon = 0.3$.

they force the disturbed flow to move down. But again, in order to satisfy the zero mass flux condition, a negative disturbance pressure gradient $\bar{\Pi}_{20}$ is induced as shown in figure 3(*d*).

In the Boussinesq limit the temperature and density disturbances, shown in figures 4(*c*) and 4(*d*), are negligible and the instability has a purely shear character. As can be seen from figure 4(*b*), the velocity disturbance tends to reduce the maximum velocity gradient and subsequently the maximum shear stress. From figure 4(*a*) we see that the disturbance also induces a weak mean horizontal velocity component which is of order ϵ, and subsequently vanishes in the Boussinesq limit ($\epsilon \to 0$). The qualitative character of the shear disturbances remains the same in the slightly and strongly non-Boussinesq regimes as can be seen from figures 5 and 6, although disturbance buoyancy effects are not negligible any more. The locations of the maximum and minimum values of the vertical component of the disturbance velocity correspond closely to the locations of disturbance density minima and maxima, respectively (see figures 5*b*, *d* and 6*b*, *d*). Consequently, the additional buoyancy effects on the disturbance tend to reduce the shear. The scaling parameter $s = \max|v_{00}|/\max|v_{20}| = \max|v_{11}|/\max|v_{20}|$ (see normalization (28)), noted in figures 4, 5 and 6 for the shear instability, decreases with ϵ, thus confirming that the relative role of the velocity disturbances becomes larger in the non-Boussinesq regimes when buoyancy effects become important.

For the buoyant mode depicted by dash-dotted lines in figure 6, the magnitude of the vertical velocity disturbance drops substantially (as indicated by the increase in scale factor). The forms of the distributions of mean flow correction quantities associated with the buoyant disturbance differ substantially from the corresponding ones associated with shear. They amplify the upward motion near the hot wall and counteract the downward motion in the neighbourhood of the cold wall. The disturbance density distribution has only one extremum, a maximum, whose position coincides with the location of the largest negative vertical velocity disturbance (see dash-dotted line on figure 6*d*). Thus, when the temperature difference between the walls exceeds the critical value of ϵ_* for Grashof numbers larger than critical a cooler region develops in the middle. Owing to its higher density, the fluid in the middle falls and thus causes the fluid closer to the walls to move up relative to it.

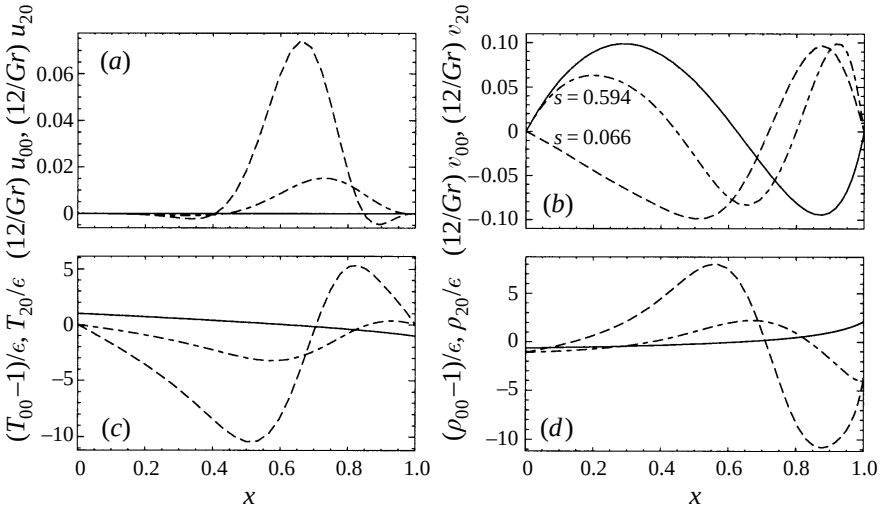

FIGURE 6. Basic flow (solid lines) and mean flow correction due to shear (dashed lines) and buoyant (dash-dotted lines) instabilities for Gr_c and the non-Boussinesq case of $\epsilon = 0.536$. The scaling parameter s is introduced for plotting purposes.

Several bifurcation diagrams for the most unstable disturbance modes at given values of ϵ are presented in figure 7(*a*). The supercritical bifurcations associated with the shear instability for the Boussinesq and slightly non-Boussinesq regimes are quite similar to each other (lines i and ii). The steepness of the bifurcation curves increases with ϵ, indicating that the disturbances in the non-Boussinesq regimes are more sensitive to a change in Grashof number. The equilibrium amplitude dependence on ϵ and on the relative distance $\delta(\epsilon) = (Gr - Gr_c(\epsilon))/Gr_c(\epsilon)$ from the bifurcation point for $\epsilon \leqslant 0.4$ is approximately given by

$$|A_e| \approx 0.20(1 + 0.11\epsilon^2 + 7.83\epsilon^4)\,\delta^{1/2}(\epsilon). \tag{82}$$

A further increase in the temperature difference leads to the appearance of the buoyant instability mode for $Gr > Gr_c$ (dash-dotted line iii). At $\epsilon = \epsilon_{**}$ the bifurcation diagram for the shear mode becomes singular (dashed line iv). This is the boundary separating regions of supercritical and subcritical bifurcations for the shear instability. At the same time the bifurcation curve for the buoyancy mode moves closer to the critical value of the Grashof number (dash-dotted line iv). Finally, at the codimension-2 point, the buoyant mode bifurcation curve meets with the one corresponding to the subcritical shear mode (line v). When the value of ϵ is increased further the buoyant instability overcomes the shear one, although as can be seen from figure 7(*a*) the two finite-amplitude disturbances can coexist in the supercritical region because of the subcritical character of the shear bifurcation (line vi). For higher values of ϵ the shear mode bifurcates at substantially larger values of the Grashof number; thus in slightly supercritical regimes one can expect the existence of only the finite buoyant disturbance (line vii). Note that the non-monotonic behaviour of the subcritical shear bifurcation curves is a reflection of the existence of a resonance between the mean flow correction and the $\alpha = 0$ harmonic for Grashof numbers smaller than the corresponding critical value for the shear instability.

From figure 7(*b*) we see that for both instabilities the wavenumber corresponding to the most rapidly growing disturbance decreases with Grashof number. From figure

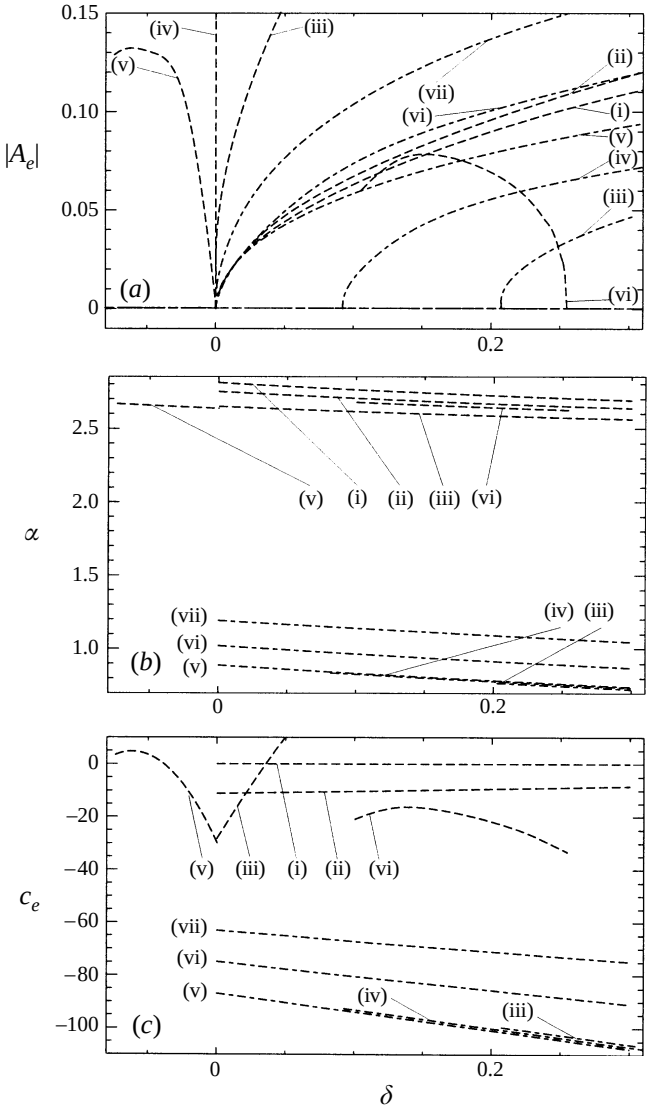

FIGURE 7. (*a*) Equilibrium amplitudes, (*b*) corresponding wavenumbers, and (*c*) equilibrium wave speeds for shear (dashed lines) and buoyant (dash-dotted lines) modes as functions of $\delta = (Gr - Gr_c)/Gr_c$ for (i) $\epsilon \ll 1$; (ii) $\epsilon = 0.3$; (iii) $\epsilon = 0.52$; (iv) $\epsilon = 0.528$; (v) $\epsilon = 0.536$; (vi) $\epsilon = 0.56$; (vii) $\epsilon = 0.6$.

7(*c*) it follows that in the Boussinesq limit the finite-amplitude disturbances do not change the stationary character of the instability since the equilibrium wave speed $c_e \equiv c_{11} - |A_e|^2 K^I/\alpha$ is zero. This is consistent with the results of Fujimura & Mizushima (1987) and Mizushima & Gotoh (1983) for $Pr = 7.5$ and the computational results of Lee & Korpela (1983) and Mizushima (1990) for $Pr = 0.71$. Since under non-Boussinesq conditions $c_{11} < 0$ and $K^I < 0$ (see figure 1*d*, *f*), the finite-amplitude shear disturbance decreases the absolute values of the wave speed in comparison with the one predicted by the linear theory. In strongly non-Boussinesq regimes, the equilibrium amplitude of the shear disturbance becomes so large (dashed line iii on figure 7*a* that the equilibrium wave speed changes its sign (dashed curve iii on figure 7*c*). This means

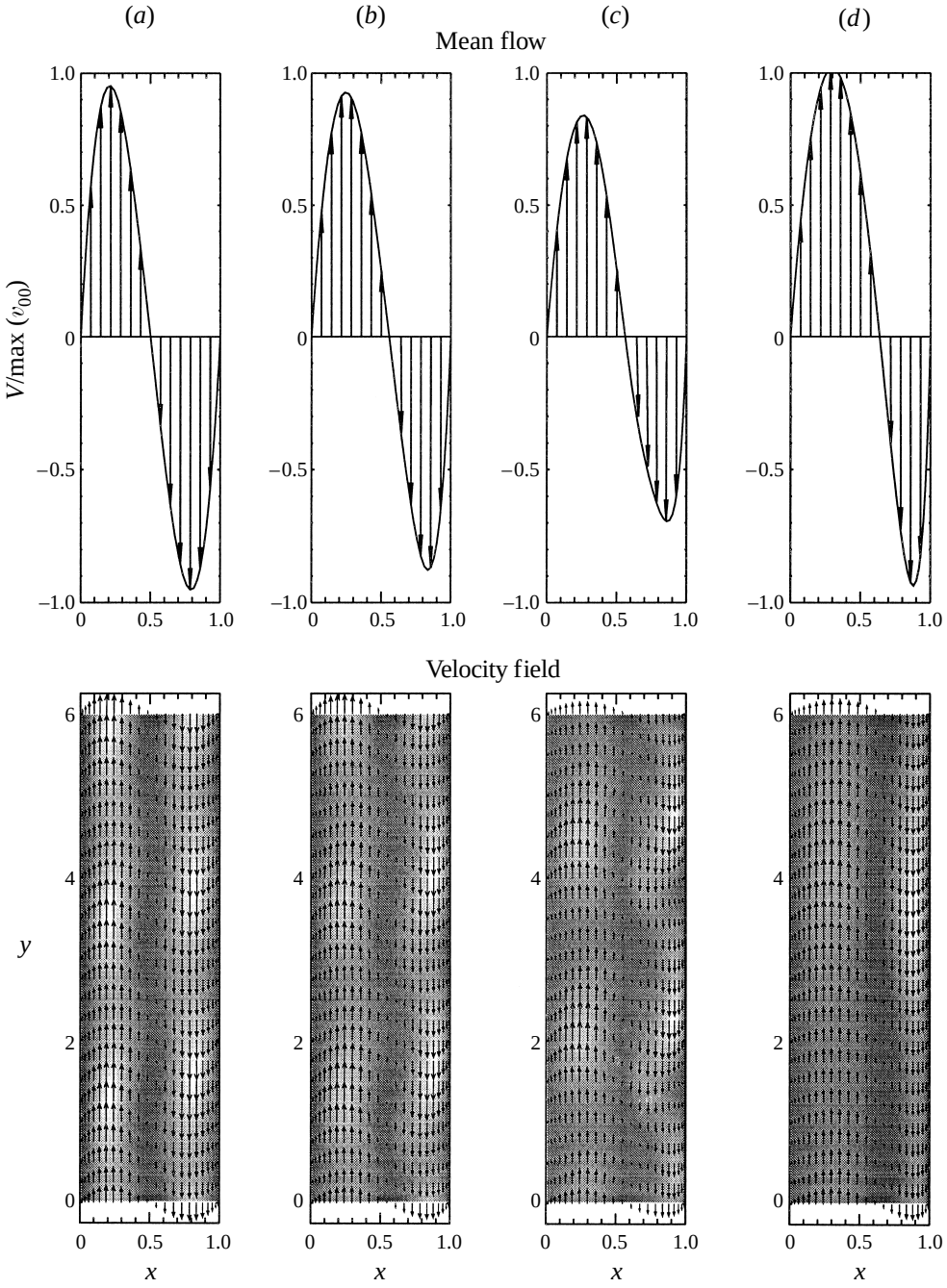

FIGURE 8. For caption see facing page.

that the growing shear disturbance is displaced from the cold wall region towards the region of upward motion closer to the hot wall. In contrast, the larger-amplitude buoyant disturbance remains located near the cold wall and moves slightly faster downward.

Finally, in figure 8, we show the instantaneous disturbed flow fields at equilibrium

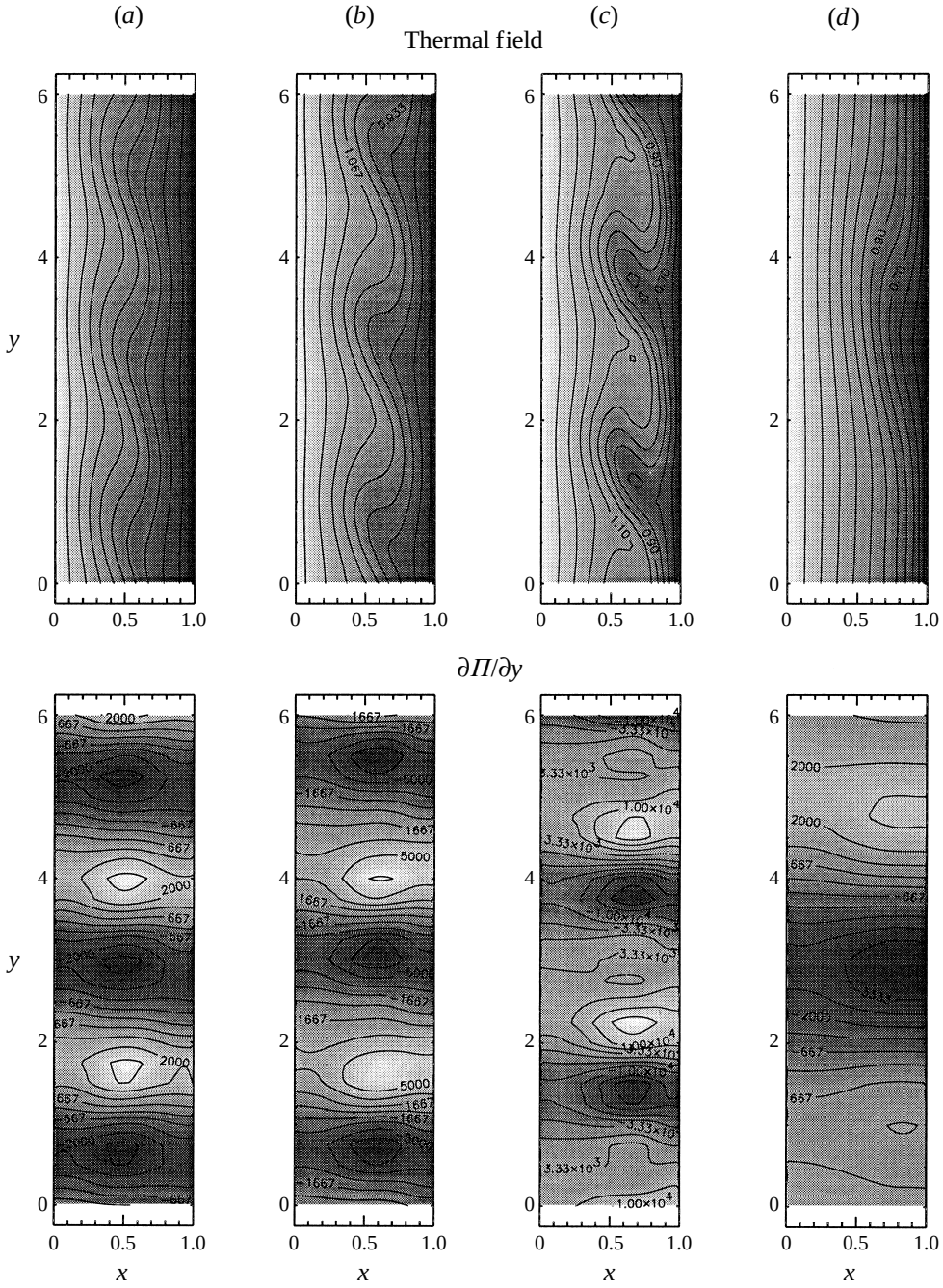

FIGURE 8. Disturbed flow for (*a*) $\epsilon \ll 1$, (*b*) $\epsilon = 0.3$, (*c*) $\epsilon = 0.5$, (*d*) $\epsilon = 0.6$, and $\delta = 0.15$.

states for supercritical regimes. All quantities are evaluated from expansions (13)–(16) truncated to second order in amplitude which can be rewritten as

$$W = w_{00}(x) + 2\,|A_e|\,|w_{11}(x)|\cos\left[\alpha(y - c_{11}\,t) + \quad(x) + \theta(t)\right] + |A_e|^2 w_{20}(x) + 2\,|A_e|^2\,|w_{22}(x)|\cos\left[2(\alpha(y - c_{11}\,t) + \quad(x) + \theta(t))\right], \quad (83)$$

	ϵ	$\ll 1$	0.3	0.536		0.6
	Instability type	Shear	Shear	Shear	Buoyant	Buoyant
$\langle E^x_{k20}\rangle$	$\langle\rho_{00}\lvert u^2_{11}\rvert\rangle$	1.525	1.526	1.424	0.221	0.417
$\langle E^y_{k20}\rangle$	$\langle\rho_{00}\lvert v^2_{11}\rvert\rangle$	3.399	3.447	3.440	3.323	3.381
	$\langle\rho_{00}v_{00}v_{20}\rangle$	−39.478	−40.830	−42.275	−0.269	1.914
	$\langle\rho_{20}v^2_{00}\rangle/2$	0.000	−0.259	−1.140	−0.285	−0.255
	$2\langle\mathrm{Re}\{\rho_{11}v^*_{11}\}v_{00}\rangle$	0.000	−0.125	−0.440	1.280	1.615
$\langle E_{k20}\rangle = \langle E^x_{k20}\rangle + \langle E^y_{k20}\rangle$		−33.029	36.211	−38.956	4.270	7.072

TABLE 1. Components of the mean disturbance kinetic energy at the critical points. All quantities are multiplied by the factor $10^5/Gr_c^2$.

where W denotes a specific dependent variable, (x) is the spatial phase variation, and

$$\theta(t) = \theta(0) + K^I \int_0^t |A(\tau)|^2 \,\mathrm{d}\tau \tag{84}$$

is the temporal phase variation which is the solution of (61). For plotting purposes we select values of time corresponding to $\theta(t) = 2\pi n$, $n = 0, \pm 1, \pm 2, \ldots$. All fields are plotted for the same range of vertical coordinate, thus one can see how the disturbance wavelength changes under non-Boussinesq conditions. The shear instability decreases the total mean flow maximum by a substantial amount under non-Boussinesq conditions. In contrast, the buoyant instability increases the maximum upward velocity. In all cases the mean flow remains essentially vertical although one can see a slightly non-parallel pattern in the middle part of the cavity in the non-Boussinesq regimes (see first row of plots in figure 8). The light (dark) areas on the plots for velocity and temperature fields correspond to the local maxima (minima) of the kinetic and thermal energy respectively (see the next subsection). We see that the location with largest kinetic energy shifts towards the cold wall as the temperature difference is increased. Simultaneously, the initially parallel flow becomes wavy due to shear disturbances. The location of the kinetic energy maximum for the buoyant mode for $\epsilon = 0.6$ coincides with the position of the dense region near the cold wall as can be seen on the plot of the thermal field. The plots in the fourth row represent the distributions of the vertical dynamic pressure gradient. Careful study of the pressure patterns indicates that the location of the negative dynamic pressure gradient (dark shaded areas) always corresponds to regions with lower temperature (and higher density). Thus, the dynamic pressure gradient always opposes the buoyant motion of the fluid and successfully dampens the buoyant instability mode for temperature differences below ϵ_*.

9.3. *Kinetic and thermal energies of the disturbed flow*

To get deeper insight into the instability physics we look at the distribution of the mean kinetic energy defined as

$$E_k + O(|A|^4) = \frac{1}{2\lambda}\int_{y_0-\lambda/2}^{y_0+\lambda/2} \rho(u^2+v^2)\,\mathrm{d}y = E_{k00} + |A|^2 E_{k20} + O(|A|^4). \tag{85}$$

We split the kinetic energy into parts associated with vertical and horizontal motions such that

$$E_{k00} = E^x_{k00} + E^y_{k00}, \quad E_{k20} = E^x_{k20} + E^y_{k20}, \tag{86}$$

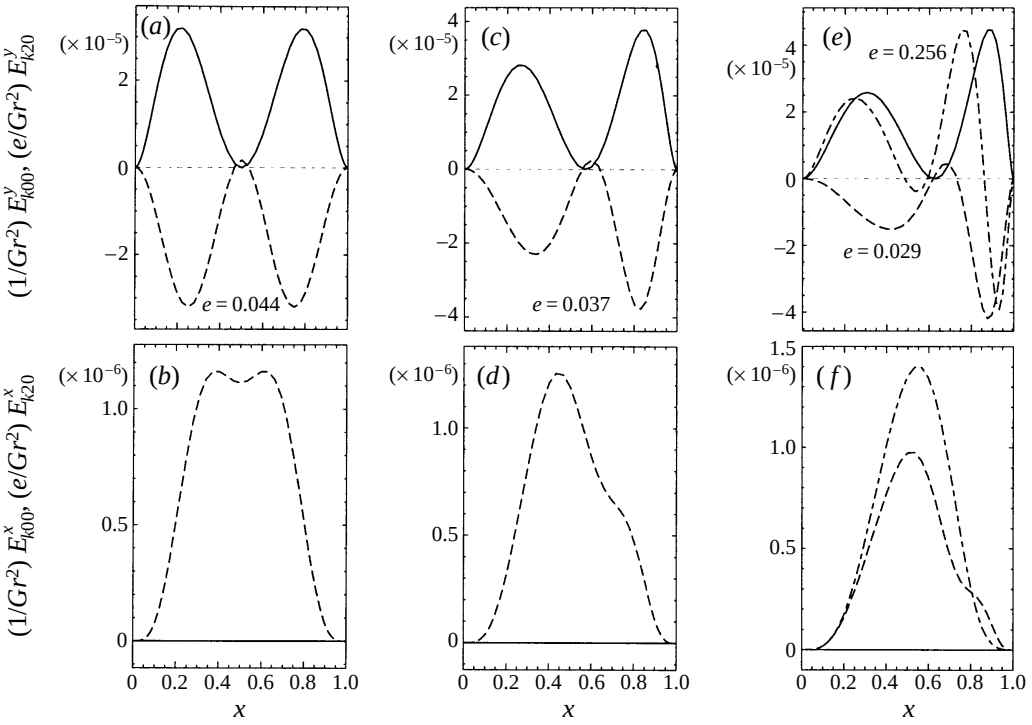

FIGURE 9. Basic flow (solid lines) and the mean flow correction kinetic energy components for shear (dashed lines) and buoyant (dash-dotted lines) instabilities for Gr_e (a, b) in the Boussinesq limit $\epsilon \ll 1$, (c, d) for $\epsilon = 0.3$, and (e, f) for $\epsilon = 0.536$. The scaling parameter e is introduced for plotting purposes.

where

$$\left.\begin{aligned} &E^x_{k00} = 0, \quad E^y_{k00} = \tfrac{1}{2}\rho_{00} v^2_{00}, \quad E^x_{k20} = \rho_{00}|u_{11}|^2, \\ &E^y_{k20} = \rho_{00}(|v_{11}|^2 + v_{00} v_{20}) + 2v_{00}\,\mathrm{Re}\{\rho_{11} v^*_{11}\} + \tfrac{1}{2}\rho_{20} v^2_{00}. \end{aligned}\right\} \tag{87}$$

It can be deduced from the linear stability results given in Suslov & Paolucci (1995*a*, *b*) that $\rho_{11} = O(\epsilon)$ as $\epsilon \to 0$. From numerical computations one can also show that $\rho_{20} = O(\epsilon)$ as $\epsilon \to 0$. Then, consistent with the classical Boussinesq results, we note that

$$\lim_{\epsilon \to 0} E^y_{k20} = (|v_{11}|^2 + v_{00} v_{20})\Big|_{\epsilon \to 0} \quad \text{since} \quad \lim_{\epsilon \to 0} \rho_{00} = 1.$$

These estimates in the Boussinesq limit are confirmed by the numerical results given in table 1. From figure 9 we see that as the temperature difference between the walls increases, the kinetic energy components associated with the vertical motion become more concentrated in the cold region. Note that similar to figures 4–6, in the non-Boussinesq regime the scaling parameter $e = \max(E^y_{k00})/\max(|E^y_{k20}|)$ decreases for the shear mode. The shear instability always tends to make the total mean kinetic energy profile more uniform, taking the energy away from the basic flow in high-speed regions near the walls and transferring it to the nearly stationary region in the middle. The energy associated with the induced horizontal motion remains an order of magnitude smaller than that associated with vertical motion. It is always concentrated in the middle part of the enclosure, although its maximum moves slightly towards the cold wall where the most energetic part of the basic flow is located when ϵ is increased.

Comparing the behaviour of the disturbance energy maxima, we can deduce that the vertical velocity disturbances are born mostly in the region with a high velocity gradient and, subsequently, a large shear stress near the cold wall. The horizontal motion is induced near the vertical midplane. The distribution of the kinetic energy associated with this motion is symmetrical in the Boussinesq regime. The symmetry is broken in non-Boussinesq regimes: the right-hand of the two maxima of figure 9(*b*) disappears almost completely as ϵ increases (see figure 9*d*,*f*), while the left-hand maximum survives, but moves further away from the hot wall.

From figure 9(*e*) we also see that the buoyancy disturbance extracts the energy from the basic flow near the cold wall and transfers it to the developing dense region closer to the middle. The left-hand negative minimum corresponds to the location where the energy is extracted from the basic flow in favour of the induced horizontal motion (see figure 9*f*) which transports the fluid from the less-dense hot region towards the denser core region.

In table 1 we illustrate the integral effect of the different disturbance components on the kinetic energy of the flow. Here the angle brackets denote integrations over the cavity width. We see that as ϵ is increased, the energy associated with the horizontal motion first increases slightly while the overall disturbance intensity becomes larger. As buoyancy begins to play a significant role, it slows down the horizontal motion leading to a more intense motion in the direction of gravity: the contribution of the buoyant disturbance to the horizontal motion is much smaller than that of the shear one. From table 1 we see that the interaction between the basic flow and the mean flow correction ($\langle \rho_{00} v_{00} v_{20} \rangle$) associated with the shear disturbance decreases the total kinetic energy $\langle E_{k20} \rangle$ of the fluid. This interaction also determines the major kinetic energy transfer mechanism for the shear instability. On the other hand, for the buoyant mode, all the components of the disturbance kinetic energy are approximately of the same order and, in contrast to the shear instability, the interaction with the disturbance density field ($\langle \rho_{20} v_{00}^2/2 + 2\,\mathrm{Re}\{\rho_{11} v_{11}^*\} v_{00} \rangle$) increases the kinetic energy of the flow.

The evolution equation for the averaged kinetic energy components can be written as

$$\frac{\partial |A|^2}{\partial t_0} \langle E_{k20} \rangle = |A|^2 \left(\langle \Sigma_{\Pi}^x \rangle + \langle \Sigma_{\Pi}^y \rangle + \frac{Gr}{2\epsilon} \langle \Sigma_B^y \rangle + \langle \Sigma_{\mu}^x \rangle + \langle \Sigma_{\mu}^y \rangle \right), \tag{88}$$

where subscripts μ, Π and B denote contributions of the viscous, pressure and buoyant forces respectively:

$$\Sigma_{\Pi}^x = -2\,\mathrm{Re}\{u_{11}^* D\Pi_{11}\}, \tag{89}$$

$$\Sigma_{\Pi}^y = 2\alpha\,\mathrm{Im}\{v_{11}^* \Pi_{11}\} - v_{00}\Pi_{20} - v_{20}\Pi_{00}, \tag{90}$$

$$\Sigma_B^y = (\rho_{00} - 1) v_{20} + \rho_{20} v_{00} + 2\,\mathrm{Re}\{\rho_{11} v_{11}^*\}, \tag{91}$$

$$\Sigma_{\mu}^x = \alpha[\tfrac{4}{3} D\mu_{00}\,\mathrm{Im}\{u_{11}^* v_{11}\} - \tfrac{2}{3}\mu_{00}\,\mathrm{Im}\{u_{11}^* Dv_{11}\} - 2\,\mathrm{Im}\{\mu_{11} u_{11}^*\} Dv_{00}] - 2\alpha^2 \mu_{00} |u_{11}|^2 + \tfrac{8}{3}\,\mathrm{Re}\{u_{11}^* D(\mu_{00} Du_{11})\}, \tag{92}$$

$$\begin{aligned} \Sigma_{\mu}^y = {} & v_{00} D(\mu_{00} Dv_{20} + \mu_{20} Dv_{00}) + v_{20} D(\mu_{00} Dv_{00}) \\ & + 2\,\mathrm{Re}\{v_{11}^* D(\mu_{00} Dv_{11} + \mu_{11} Dv_{00}) + v_{00} D(\mu_{11} Dv_{11}^*)\} \\ & + 2\alpha\,\mathrm{Im}\{D\mu_{00} u_{11}^* v_{11} - \tfrac{1}{3}\mu_{00} Du_{11}^* v_{11} + D(\mu_{11} u_{11}^*) v_{00}\} - \tfrac{4}{3}\mu_{00} |v_{11}|^2. \end{aligned} \tag{93}$$

The different components of the disturbance kinetic energy balance equations obtained

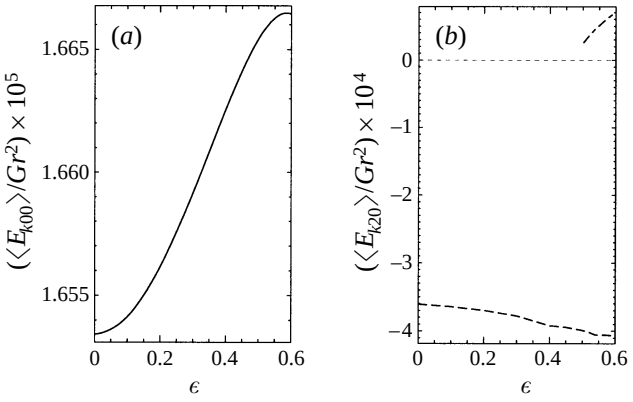

FIGURE 10. The average kinetic energy for (*a*) the basic flow (solid lines) and (*b*) shear (dashed lines) and buoyant (dash-dotted lines) disturbances evaluated at the critical points as functions of ϵ.

ϵ	$\ll 1$	0.3	0.536		0.6
Instability type	Shear	Shear	Shear	Buoyant	Buoyant
$\langle \Sigma^x_\mu\rangle/\langle E_{k20}\rangle$	2.25	2.21	2.03	−1.97	−2.31
$\langle \Sigma^x_\Pi\langle/\langle E_{k20}\rangle$	−2.25	−2.21	−2.03	1.97	2.31
$\langle \Sigma^y_\mu\rangle/\langle E_{k20}\rangle$	−71.8	−71.7	−72.0	−42.0	−44.8
$\langle \Sigma^y_\Pi\rangle/\langle E_{k20}\rangle$	2.3	1.5	−0.7	1.5	−1.3
$Gr/(2\epsilon)\langle \Sigma^y_B\rangle/\langle E_{k20}\rangle$	69.5	70.2	72.7	40.4	46.1

TABLE 2. Terms entering the averaged kinetic energy evolution equation and evaluated at the critical points.

for various values of the temperature difference are given in table 2. From there we deduce that: (*a*) the viscous dissipation always tends to reduce the modulus of the unsteady disturbance amplitude since the viscous terms contribute negatively to the kinetic energy balance, (*b*) the only force inducing the horizontal motion is the horizontal pressure gradient Σ^x_Π, and (*c*) the integral role of the vertical pressure gradient Σ^y_Π is minor in comparison with the buoyancy force Σ^y_B which is primarily responsible for the growth of the kinetic energy of the vertical component of the disturbed motion.

In concluding the disturbance kinetic energy study we note from figure 10(*a*) that the basic flow motion becomes slightly more energetic when the temperature difference between the walls increases. From figure 10(*b*) we see that the developing shear disturbances tend to reduce the total kinetic energy ($\langle E_{k20}\rangle < 0$). In contrast, from the same figure, we see that the buoyant disturbance increases the flow kinetic energy slightly.

The mean thermal energy of the fluid in the cavity is given by

$$E_t + O(|A|^4) = \frac{1}{\lambda}\int_{y_0-\lambda/2}^{y_0+\lambda/2} \rho c_v T \,\mathrm{d}y = E_{t00} + |A|^2 E_{t20} + O(|A|^4), \tag{94}$$

where

$$E_{t00} = \frac{1}{\gamma_r}\rho_{00} T_{00} = \frac{P_{00}}{\gamma_r}, \quad E_{t20} = \frac{1}{\gamma_r}(\rho_{20} T_{00} + \rho_{00} T_{20} + \mathrm{Re}\{\rho_{11} T^*_{11}\}) = \frac{P_{20}}{\gamma_r} \tag{95}$$

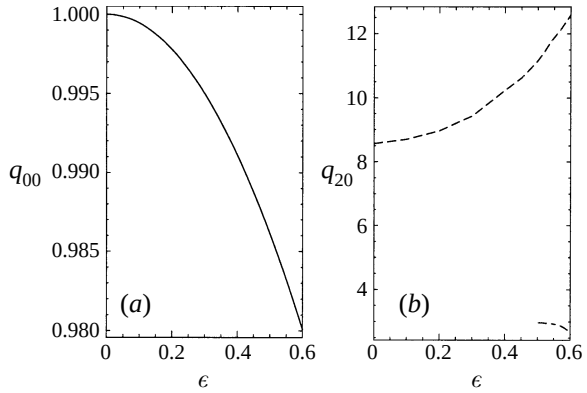

FIGURE 11. The average heat flux for (*a*) the basic flow and (*b*) disturbances at critical points for the shear (dashed line) and buoyant (dash-dotted lines) disturbances as functions of ϵ.

and according to figure 3(*b*) both shear and buoyant instabilities diminish the total mean thermal energy of the fluid in the cavity.

Note that since the vertical walls of the cavity are conducting, the fluid in the cavity can exchange the energy with the ambient during the transient period. This energy exchange is more intense when the instability is driven by shear since in this case both the thermal energy and the kinetic energy of the fluid are decreased by the developing disturbance. In the buoyant instability case part of the thermal energy is converted to the kinetic energy and does not leave the enclosure, thus the change with the ambient is less intense.

9.4. *Heat transfer*

Another important characteristic of the flow is the heat flux across the cavity. In dimensionless form this is given by the Nusselt number

$$Nu = \frac{1}{q_c}\left[\frac{1}{\lambda}\int_{y_0-\lambda/2}^{y_0+\lambda/2} q\,\mathrm{d}y\right]_{x=1} = 1+|A_c|^2\left.\frac{q_{20}}{q_{00}}\right|_{x=1} \tag{96}$$

which is a ratio of the average heat flux to the conduction heat flux. In (96) we recognize that the conduction heat flux is

$$q_c = q_{00} = -\frac{1}{2\epsilon}k_{00}\,DT_{00} \tag{97}$$

and it decreases with ϵ in accordance with the Taylor series expansion of the basic flow solution as

$$\begin{aligned} q_{00} &= 1-\frac{1}{24}\frac{1+6S_k-3S_k^2}{(1+S_k)^2}\epsilon^2-\frac{1}{640}\frac{5+60S_k-9S_k^2-20S_k^3-3S_k^4}{(1+S_k)^4}\epsilon^4+O(\epsilon^6)\\ &\approx 1-0.056\epsilon^2-0.007\epsilon^4 \end{aligned} \tag{98}$$

and is shown on figure 11(*a*). The convective component of the average heat flux, which is associated with the disturbance field, is given by

$$q_{20} = -\frac{1}{2\epsilon}k_{00}\,DT_{20}\bigg|_{x=1}. \tag{99}$$

For $Gr = Gr_c(\epsilon)$ this quantity is shown in figure 11(*b*). A curve fit of these data for $\epsilon \leqslant 0.4$ gives

$$q_{20}\,|_{\delta(\epsilon)=0} = 8.56(1+1.02\epsilon^2+1.14\epsilon^4). \tag{100}$$

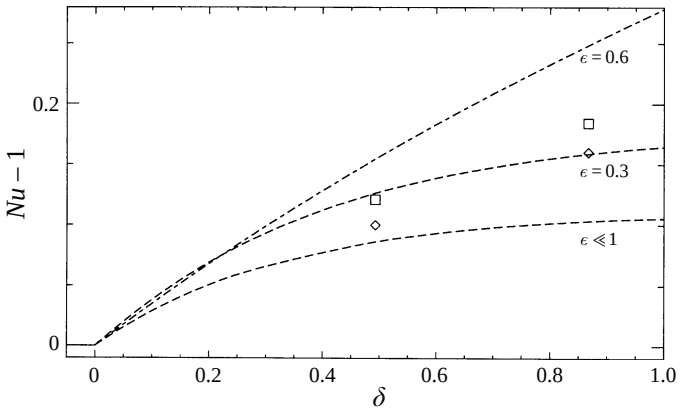

FIGURE 12. Nusselt number as a function of δ for different ϵ. Dashed and dash-dotted lines denote contributions of the shear- and buoyancy-driven instabilities respectively. Symbols denote results of the direct numerical simulation for free convection of air in a cavity of aspect ratio 20 computed in the Boussinesq limit in Lee & Korpela (1983) (diamonds) and Mizushima (1990) (squares).

From the figure we see that the convective component of heat transfer increases rapidly with ϵ owing to the development of disturbances associated with shear, while the contribution from the buoyant mode, although also positive, decreases as the temperature difference between the walls increases.

Combining (82) with (98) and (100), for slightly supercritical regimes we obtain

$$(Nu-1)/\delta(\epsilon) \approx 0.34 - 0.44\epsilon^2 + 5.77\epsilon^4. \tag{101}$$

Relationships of similar type, $(Nu-1)/\delta = a$, derived from quasi-linear theory were reported for free and mixed convection Boussinesq flows in Gotoh & Ikeda (1972) and Fukui *et al.* (1982), although the values of the correlation constant a (0.4551 and 0.6508 respectively) in those works differ substantially from the present result (0.34). Equation (101), in fact, gives the slope of the Nusselt number curve for fixed ϵ as $\delta \to 0$. The actual behaviour of the average Nusselt number for finite values of δ deviates from the linear relationship, as illustrated in figure 12. The average Nusselt number (96) is proportional to the disturbance amplitude squared. On the other hand, q_{20} (see (99)) decreases with δ and thus the Nusselt number deviates from linear dependence on δ. This was also demonstrated in Mizushima & Gotoh (1983) for $Pr = 7.5$. We compare the values of Nu predicted in the Boussinesq regime by the present analysis with those obtained by direct numerical simulations of free convection of air in a cavity of aspect ratio 20 in Lee & Korpela (1983) and Mizushima (1990) for $\delta = 0.5$ and $\delta = 0.89$. The weakly nonlinear theory predicts values of Nusselt numbers which are 3–6% below the computational results. This is easily explained if one recalls that in this work the instability is modelled by a single mode, while a finite band of disturbances contributes to the convective heat flux in the numerical simulations. From figure 12 it also can be seen that non-Boussinesq effects intensify the convective heat transfer associated with shear and buoyant disturbances.

9.5. *Two-mode interactions*

Numerical evaluations for the codimension-2 point give $\mu_1 = \mu_2 = 0$, $b = 10.836$, $c = -1.401$ and $d = -1$ (see (79) for definitions). This situation corresponds to Type 1c (saddle point with two invariant lines $r_1 = 0$ and $r_2 = 0$) according to the classification of degenerate fixed points given by Guckenheimer & Holmes (1983).

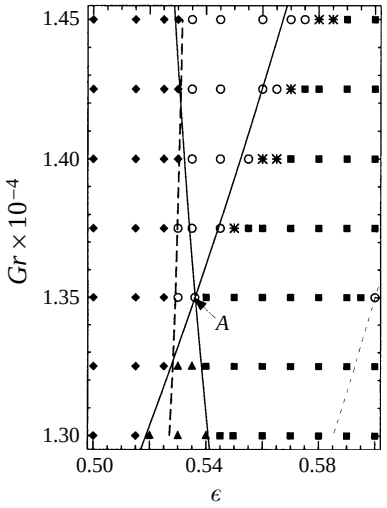

	Instability type	
	Shear	Buoyant
Diamond	$\lvert A_{1e}\rvert > 0$	$\lvert A_{2e}\rvert = 0$
Square	$\lvert A_{1e}\rvert = 0$	$\lvert A_{2e}\rvert > 0$
Star	$\lvert A_{1e}\rvert > 0$	$\lvert A_{2e}\rvert > 0$
Triangle	$\lvert A_{1e}\rvert = 0$	$\lvert A_{2e}\rvert = 0$
Circle	No stable equilibrium found	

FIGURE 13. Two-mode interaction diagram. The solid lines denote the boundary of linear stability for shear and buoyant modes (see also figure 1*a*). The shear instability bifurcation is subcritical to the right of the dashed line. The mean flow correction for the shear mode resonates with the $\alpha = 0$ harmonic along the dotted line.

Stable equilibria of different types can exist in the neighbourhood of the codimension-2 point A shown in figure 13. Before we discuss these results we should recall that the present analysis is able to predict only the existence of a subcritical bifurcation to the right of the dashed line. A stable equilibrium for the subcritical bifurcation is reached at substantially larger values of amplitude. Consequently, its determination would require a higher-order expansion which is beyond the scope of the present work. For this reason no stable equilibria were found in the region marked by circles. The interaction of the two instability modes does not affect the basic flow in the linearly stable regions: the only stable equilibria found there correspond to the zero-amplitude pair. The interaction of the modes does not lead to their asymptotic coexistence in the majority of the cases either: in most of the regions only one, linearly unstable, mode ultimately survives. The characteristics of the two disturbances (wavenumbers and wave speeds) are so different that the coupling between them does not affect the asymptotic behaviour except in the region in figure 13 marked by stars. There, mixed-mode disturbances are found to define the resulting flow. This region is below the linear stability curve for the shear mode, indicating that the subcritical bifurcation plays an important role even for small amplitudes. The dashed line in the lower right corner of figure 13 denotes the points where our expansions are not uniformly valid due to resonance between the mean flow correction and the $\alpha = 0$ shear disturbance wave. Consideration of such a resonance would require a three-mode analysis and, possibly, higher-order expansions in order to find the equilibrium for the subcritical bifurcation associated with the shear mode. Owing to the highly nonlinear character of the governing equations, this would lead to an extremely complex algebraic problem. We will treat the analysis of the flow in these regions by direct numerical simulation which will be carried out in the future.

In figure 14 we present the evolution of two-mode interactions in phase space. It is found that phase patterns for the points located to the left and the right of the dashed line in figure 13 are topologically equivalent to Cases II (figure 14*a*, *b*, *e*) and VIa (figure 14*c*, *d*, *f*, *g*, *h*), respectively, as classified by Guckenheimer & Holmes (1983) by

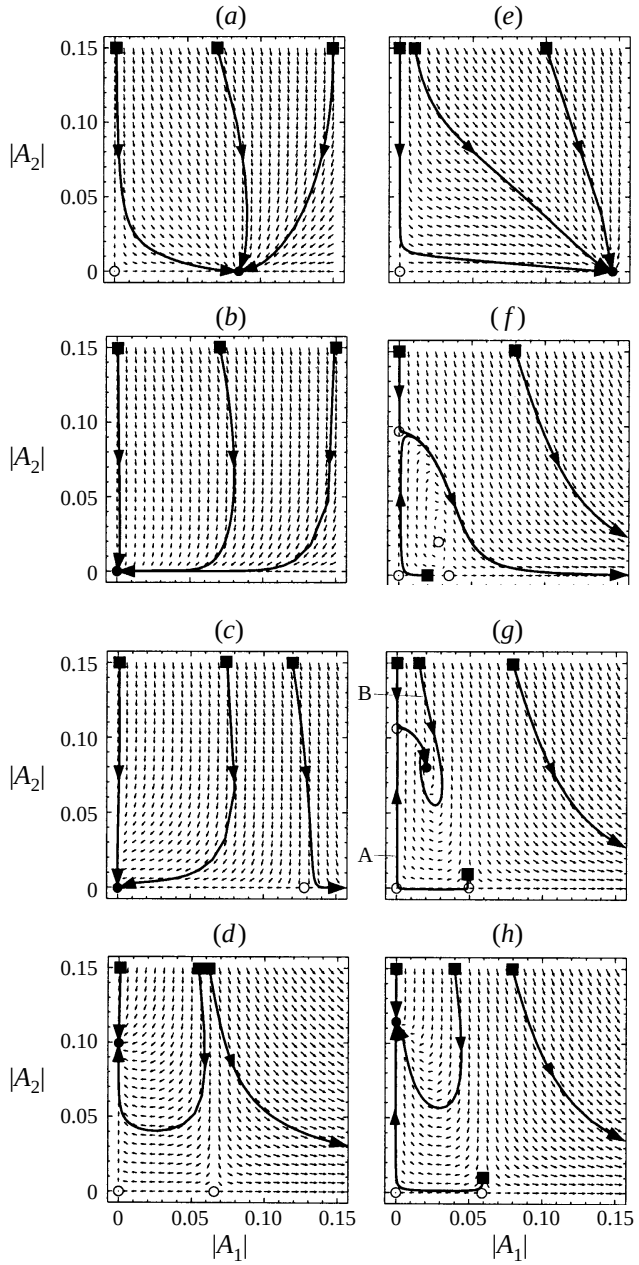

FIGURE 14. Amplitude flow diagrams for $Gr = 13\,000$ (left-hand column) and $Gr = 14\,000$ (right-hand column) and (*a*) $\epsilon = 0.500$, (*b*) $\epsilon = 0.520$, (*c*) $\epsilon = 0.535$, (*d*) $\epsilon = 0.570$, (*e*) $\epsilon = 0.500$, (*f*) $\epsilon = 0.555$, (*g*) $\epsilon = 0.560$, and (*h*) $\epsilon = 0.570$. The solid lines represent amplitude trajectories. Filled and open circles denote the stable equilibria and saddle points respectively. Squares represent initial conditions.

examining the unfoldings from the degenerate fixed point. Although we do not show it here, we note that all flow patterns distinguished by Guckenheimer & Holmes for Case VIa, including homoclinic orbits, exist in the vicinity of the codimension-2 point.

For Grashof numbers below the value corresponding to the codimension-2 point (figure 14*a–d*) the two modes cannot reach a stable finite-amplitude state sim-

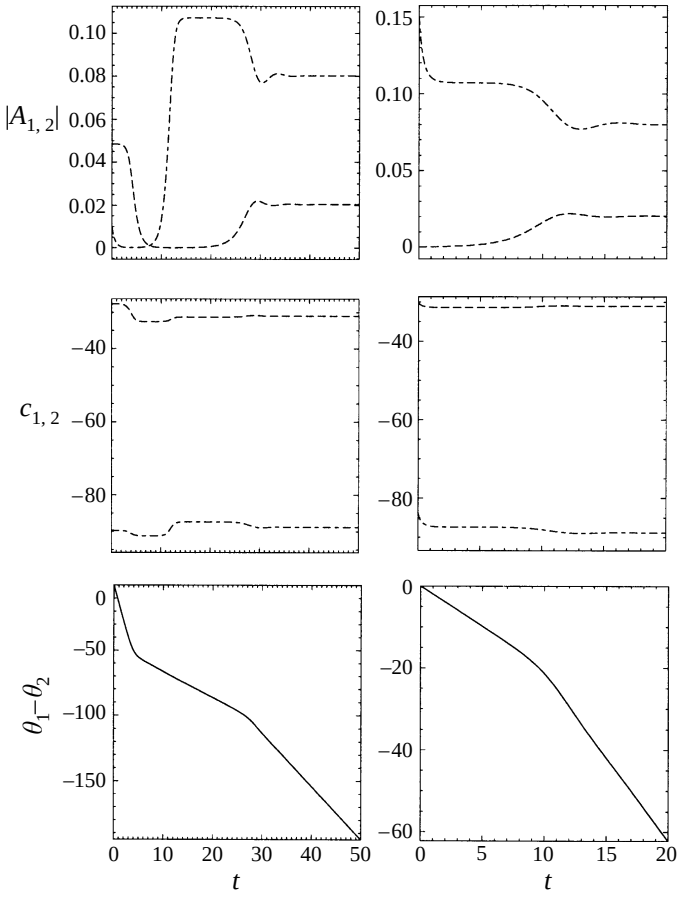

FIGURE 15. Evolution of amplitudes, wave speeds, and phase difference for trajectories A (left-hand column) and B (right-hand column) in figure 14(*g*). Dashed and dash-dotted lines correspond to shear and buoyant modes respectively.

ultaneously. For smaller values of ϵ (plot *a*) the shear disturbance, being linearly unstable, reaches a stable finite equilibrium, while the buoyant one rapidly decays regardless of the initial conditions. The case when the basic flow is linearly stable with respect to both disturbances is shown in plots (*b*) and (*c*). Comparing these two plots we see that the subcriticality of the shear bifurcation introduces a saddle point (plot *c*). The basic flow becomes conditionally stable since the shear disturbance can decay only for an initial amplitude below a certain value. Further increase of the temperature difference between the walls destabilizes the basic flow with respect to the buoyant disturbances. The shear disturbance does not affect the asymptotic state unless its initial amplitude is greater than some threshold. In the latter case the shear instability becomes dominant although the basic flow is linearly stable with respect to shear disturbances. If $Gr < Gr_c(\epsilon_*)$ and we are far enough from equilibrium, from figure 14(*a–d*) we see that the shear disturbance always dominates over the buoyant one even when the latter is growing according to the linear analysis (the vertical flow towards zero prevails in the amplitude trajectories).

The interaction between the shear and buoyant disturbances for $Gr > Gr_c(\epsilon_*)$ in the supercritical region (between the two solid lines on figure 13) destabilizes all equilibria (figure 14*f*). As in the case of smaller ϵ the shear disturbance dominates over the

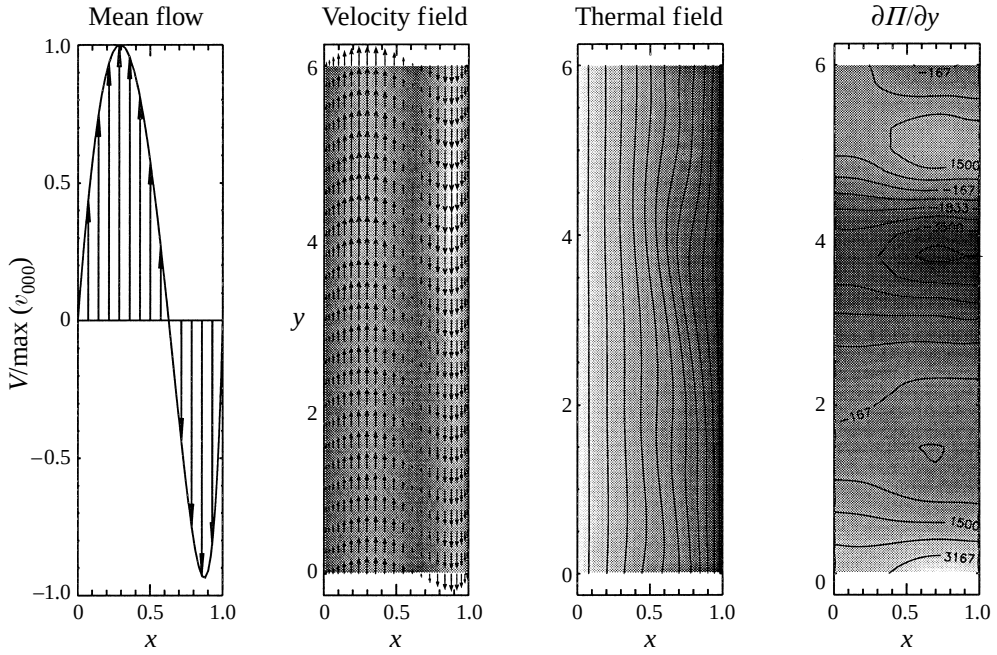

FIGURE 16. Disturbed flow for the mixed instability mode at $\epsilon = 0.56$, and $Gr = 14000$.

buoyant one causing its fast decay with time. It is expected that this shear mode will saturate with inclusion of higher-order terms in amplitude in the analysis. For larger values of ϵ and farther from the critical stability curve (see figure 13) the buoyant mode becomes sufficiently strong to overcome the influence of the shear mode. As a result, a mixed disturbance exists as shown in figure 14(*g*). Further increase of the temperature difference diminishes the relative role of the shear mode and its equilibrium amplitude vanishes (see figure 14(*h*). Comparing figure 14(*a* and *e*) and (*d* and *h*) we see that they are qualitatively similar to each other and consequently we conclude that the character of the phase portrait away from the codimension-2 point is defined only by the distance from the respective critical points.

The path along which the disturbances approach their asymptotic states as well as the time necessary to reach them depend strongly on the initial conditions. Two possible scenarios corresponding to trajectories A and B in figure 14(*g*) are depicted in figure 15. Trajectory A shows that the initially interacting finite disturbances in the linearly unstable region can decay rapidly at first to very small values. This would at first appear to be counterintuitive from a linear analysis standpoint. However, linear analysis only tells us about asymptotic behaviour. The disturbances also can approach the unstable equilibria and stay there for a substantial time before they finally reach the stable equilibrium. For a different choice of initial conditions corresponding to trajectory B in figure 14, the amplitude of the subcritical shear mode decays exponentially at first, while the supercritical buoyant disturbance grows exponentially. After some oscillations, the amplitudes eventually settle to their asymptotic values. As the disturbances develop, the wave speeds corresponding to the shear and buoyant modes change slightly but remain substantially different. Because of this, the phase difference $\theta_1 - \theta_2$ between the shear and buoyant modes is always negative and its absolute value increases rapidly with time. Thus no phase locking is observed between

Type of flow	Saturation amplitudes	Stability of equilibrium	E^x_{k20}	E^y_{k20}	E_k	E_{t20}	E_t
Basic flow	$\begin{cases} \lvert A_1\rvert_e = 0.000, \\ \lvert A_2\rvert_e = 0.000 \end{cases}$	Unstable	0.0	0.0	3266.1	0.000	0.708
Buoyant disturbance	$\begin{cases} \lvert A_1\rvert_e = 0.000, \\ \lvert A_2\rvert_e = 0.107 \end{cases}$	Unstable	5.2	90.6	3361.9	−0.010	0.698
Shear disturbance	$\begin{cases} \lvert A_1\rvert_e = 0.048, \\ \lvert A_2\rvert_e = 0.000 \end{cases}$	Unstable	6.4	−194.0	3078.5	−0.003	0.705
Mixed disturbance	$\begin{cases} \lvert A_1\rvert_e = 0.020, \\ \lvert A\rvert_e = 0.080 \end{cases}$	Stable	4.0	17.0	3287.1	−0.006	0.702

TABLE 3. Mean kinetic and thermal energies at the different equilibrium states for the representative point $(\epsilon, Gr) = (0.56, 14000)$.

the two modes. Since the phase shift between the two modes changes constantly the flow pattern corresponding to the mixed disturbance also changes with time. For simplicity, on figure 16 we illustrate the disturbed flow at the representative point $(\epsilon, Gr) = (0.56, 14000)$ shown in figure 14(f) at a particular moment when $\theta_1 = 2\pi m$ and $\theta_2 = 2\pi n$, where m and n are integers. Comparison with figure 8(d) shows that the form of the mixed disturbance is close to that of the buoyant mode while the shear disturbance slightly increases the waviness of the resulting flow.

Finally, we analyse the effect of the two modes on the mean kinetic energy of the flow at the same representative point. The components of the kinetic and thermal energies computed using definitions (85)–(86) and (94)–(95) are given in table 3. The basic flow becomes unstable due to the buoyancy disturbance (see trajectory A). This disturbance reaches its unstable equilibrium amplitude value of 0.107 and thus increases the total kinetic energy of the flow. Owing to its subcritical character, the shear disturbance begins to develop at that point. It tends to reach saturation at the amplitude value of 0.048, leading to a decreasing amplitude of the buoyancy mode and to dissipation of mean flow kinetic energy. The two modes equilibrate at some intermediate values of amplitudes, resulting in a slight increase in the mean flow kinetic energy. Thus, we conclude that the existence of the stable finite-amplitude equilibrium for all modes is closely related to the disturbance energy production–dissipation balance associated with the different instability mechanisms. Note also that the buoyant, shear and mixed disturbances decrease the thermal energy of the fluid and that, in contrast to the Boussinesq limit, the relative change of the fluid thermal energy is of the same order as that of the kinetic energy for the non-Boussinesq regimes.

10. Conclusions

A weakly nonlinear theory is developed for flows described by the equations having general nonlinearity. The theory is applied to the natural convection flow of air in a tall differentially heated closed cavity for a wide range of Grashof numbers and temperature differences. The flow is appropriately described by the low-Mach-number equations. It is found that for small temperature differences the basic flow bifurcates supercritically due to shear-driven disturbances. This bifurcation becomes subcritical for larger temperature differences. In strongly non-Boussinesq regimes, the buoyant disturbances become important and lead to a supercritical bifurcation of the basic flow. The two disturbances compete with each other and both can reach finite asymptotic

equilibrium amplitudes for a certain range of Gr and $\epsilon > \epsilon_*$. Detailed energy analysis of the disturbed flow shows that the two disturbances have an opposite influence on the mechanical energy of the flow, although both of them decrease the thermal energy of the fluid in the cavity.

This work was partially sponsored by a fellowship from the Center for Applied Mathematics of the University of Notre Dame.

Appendix A

Let us consider the problem

$$\mathrm{N}(\boldsymbol{W}-\boldsymbol{W}_0;\sigma)=0, \quad \mathrm{N}(\mathbf{0};\sigma)=0, \tag{A 1}$$

where N is a nonlinear operator and σ is some complex parameter. For small deviations $\Delta\boldsymbol{W}=\boldsymbol{W}-\boldsymbol{W}_0$, after applying a Taylor series expansion, the general nonlinear problem becomes

$$\mathrm{N}(\Delta\boldsymbol{W};\sigma)=\sum_{k=1}^{\infty}\mathrm{N}_k(\Delta\boldsymbol{W};\sigma)=\sum_{k=1}^{\infty}\sum_{i=1}^{I_k}\prod_{l=1}^{k}\mathrm{L}_l^{(i)}(\Delta\boldsymbol{W};\sigma), \tag{A 2}$$

where $\mathrm{L}_l^{(i)}$ are linear operators such that $\mathrm{L}_l^{(i)}(\mathbf{0};\sigma)=0$, and I_k is their total number which is specified for each k for a particular problem. Substituting expansion (11) into (A 2) we obtain

$$\begin{aligned}
\mathrm{N}(\Delta\boldsymbol{W};\sigma) &= \sum_{k=1}^{\infty}\sum_{i=1}^{I_k}\prod_{l=1}^{k}\mathrm{L}_l^{(i)}\left(\sum_{m=1}^{\infty}\sum_{n=-\infty}^{\infty}\varepsilon^m E^n\hat{\boldsymbol{w}}_{mn};\sigma\right)\\
&= \sum_{k=1}^{\infty}\sum_{i=1}^{I_k}\prod_{l=1}^{k}\left[\sum_{m=1}^{\infty}\sum_{n=-\infty}^{\infty}\varepsilon^m E^n\mathscr{L}_l^{(i)}(\hat{\boldsymbol{w}}_{mn};\sigma,n\alpha)\right]\\
&= \sum_{k=1}^{\infty}\sum_{i=1}^{I_k}\sum_{m=1}^{\infty}\sum_{n=-\infty}^{\infty}\varepsilon^m E^n\sum_{\sum_{p=1}^{k}m_p=m,\ \sum_{q=1}^{k}n_q=n}\prod_{l=1}^{k}\mathscr{L}_l^{(i)}(\bar{\boldsymbol{w}}_{m_pn_q};\sigma,n_q,\alpha)\\
&= \sum_{m=1}^{\infty}\sum_{n=-\infty}^{\infty}\varepsilon^m E^n\sum_{k=1}^{\infty}\sum_{\sum_{p=1}^{k}m_p=m,\ \sum_{q=1}^{k}n_q=n}\sum_{i=1}^{I_k}\prod_{l=1}^{k}\mathscr{L}_l^{(i)}(\hat{\boldsymbol{w}}_{m_pn_q};\sigma,n_q\alpha)\\
&= \sum_{m=1}^{\infty}\sum_{n=-\infty}^{\infty}\varepsilon^m E^n\sum_{k=1}^{\infty}\sum_{\sum_{p=1}^{k}m_p=m,\ \sum_{q=1}^{k}n_q=n}\mathscr{N}_k(\hat{\boldsymbol{w}}_{m_pn_q};\sigma,n_q\alpha)=0,
\end{aligned} \tag{A 3}$$

where $\mathscr{N}_k$ is a nonlinear operator of kth order. Then for the $\varepsilon^m E^m$ we have

$$\begin{aligned}
\mathscr{N}_1(\hat{\boldsymbol{w}}_{mn};\sigma,n\alpha) &\equiv \mathscr{L}(\hat{\boldsymbol{w}}_{mn};\sigma,n\alpha)\\
&\equiv \sum_{i=1}^{I_1}\mathscr{L}_1^{(i)}(\hat{\boldsymbol{w}}_{mn};\sigma,n\alpha)\\
&= -\sum_{k=2}^{\infty}\sum_{\sum_{p=1}^{k}m_p=m,\ \sum_{q=1}^{k}n_q=n}\mathscr{N}_k(\hat{\boldsymbol{w}}_{m_pn_q};\sigma,n_q\alpha),
\end{aligned} \tag{A 4}$$

where we note that $\mathscr{N}_1$ is a linear operator.

Note 1. At order $\varepsilon^1E^{\pm1}$ we have

$$\mathscr{L}(\hat{\boldsymbol{w}}_{1\pm1};\sigma,\pm\alpha)=0. \tag{A 5}$$

This is an eigenvalue problem with generally complex eigenvalue σ and eigenvectors $\hat{\boldsymbol{w}}_{1\pm1}$ for a fixed wavenumber α.

Note 2. If the sum on the right-hand side of (A 4) is zero, then (A 4) only has the trivial solution provided that σ, defined by eigenvalue problem (A 5), is not an eigenvalue of

$$\mathscr{L}(\hat{\boldsymbol{w}}_{mn};\sigma,n\alpha)=0. \tag{A 6}$$

LEMMA *If for $m<2$ the only non-zero terms in expansion* (11) *satisfying problem* (*A* 1) *are $\hat{w}_{00}$, $\hat{w}_{11}$, and $\hat{w}_{1-1}$, and σ is not the eigenvalue of problems* (*A* 6) *for $m>1$, then for all $m>1$, $\hat{w}_{mn}\not\equiv 0$ only if $m+n$ is even and $|n|\leqslant m$.*

Proof Let $\hat{\boldsymbol{w}}_{ij}\not\equiv 0$ if $\{(-1)^{i+j}=1,\ |j|\leqslant i\}$ for all i such that $0<i<m$. Under the assumptions of the lemma, it follows from (A 4) that for $k=2,3,\ldots,$

$$m+n=\sum_{p=1}^{k}i_p+\sum_{q=1}^{k}j_q=\sum_{s=1}^{k}\underbrace{(i_s+j_s)}_{\text{even}}=\text{even}, \tag{A 7}$$

and

$$\max(|n|-m)=\max\left(\left|\sum_{q=1}^{k}j_q\right|-\sum_{p=1}^{k}i_p\right)\leqslant\max\left(\sum_{s=1}^{k}(|j_s|-i_s\right)=0, \tag{A 8}$$

where we have used the triangle inequality.

For $m=2$ we have from (A 4)

$$\left.\begin{aligned}
n=0:&\quad \mathscr{L}(\hat{\boldsymbol{w}}_{20};\sigma,0)=-\mathscr{N}_2(\hat{\boldsymbol{w}}_{11},\hat{\boldsymbol{w}}_{1-1};\sigma,0),\\
|n|=1:&\quad \mathscr{L}(\hat{\boldsymbol{w}}_{2\pm1};\sigma,\pm\alpha)=0,\\
|n|=2:&\quad \mathscr{L}(\hat{\boldsymbol{w}}_{2\pm2};\sigma,\pm2\alpha)=-\mathscr{N}_2(\hat{\boldsymbol{w}}_{1\pm1},\hat{\boldsymbol{w}}_{1\pm1};\sigma,\pm2\alpha),\\
|n|>2:&\quad \mathscr{L}(\hat{\boldsymbol{w}}_{2n};\sigma,n\alpha)=0.
\end{aligned}\right\} \tag{A 9}$$

We note that for $|n|=1$ we obtain the same eigenvalue problem as (A 5), thus $\hat{\boldsymbol{w}}_{2\pm1}=\hat{\boldsymbol{w}}_{1\pm1}$. Since ε is just a formal expansion parameter, we can redefine $\varepsilon+\varepsilon^2\to\varepsilon$ such that $(\varepsilon\hat{\boldsymbol{w}}_{1\pm1}+\varepsilon^2\hat{\boldsymbol{w}}_{2\pm1})E^{\pm1}=(\varepsilon+\varepsilon^2)\hat{\boldsymbol{w}}_{1\pm1}E^{\pm1}\to\varepsilon\hat{\boldsymbol{w}}_{1\pm1}E^{\pm1}$. Effectively this means that without any loss of generality we can take $\hat{\boldsymbol{w}}_{2\pm1}\equiv 0$. Next, using *Note* 2, we conclude that $\hat{\boldsymbol{w}}_{2n}\not\equiv 0$ only if $2+n$ is even and $|n|\leqslant 2$. Repeating the above argument for $m=3,4,\ldots,$ we prove the lemma by induction. □

We further assume that $\hat{\boldsymbol{w}}_{mn}$ can be written in the separable form

$$\hat{\boldsymbol{w}}_{mn}=f_{mn}(A,|A|)\,\boldsymbol{w}_{mn}(x),\quad f_{m-n}=f^*_{mn},\quad \boldsymbol{w}_{m-n}=\boldsymbol{w}^*_{mn}, \tag{A 10}$$

where $\varepsilon A=O(\varepsilon)$ and A depends only on time. Taking into account the polynomial character of the nonlinearity in the problem, it is convenient to choose $f_{mn}=A^p|A|^q$, $p,q\geqslant 0$, such that $p+q=m$ and $p=n$, or

$$f_{mn}=\begin{cases}A^n|A|^{m-n}, & n\geqslant 0\\ (A^*)^{-n}|A|^{m+n}, & n<0.\end{cases} \tag{A 11}$$

Subsequently we rewrite expansion (11) in the form

$$\boldsymbol{W}=\sum_{k=0}^{\infty}\varepsilon^{2k}|A|^{2k}\boldsymbol{w}_{2k0}+\sum_{m=1}^{\infty}\sum_{k=0}^{[2m-3-(-1)^m]/4}\varepsilon^m|A|^{m-n}[(AE)^n\boldsymbol{w}_{mn}+\text{c.c.}], \tag{A 12}$$

where $n=2k+[3+(-1)^m]/2$, and c.c. denotes the complex conjugate. The first and second sums represent a non-periodic mean flow and periodic disturbance modes respectively.

Appendix B

Elements of $(\boldsymbol{A}_\alpha)_{m,n} = (a_2)_{m,n} D^2 + (a_1)_{m,n} D + (a_0)_{m,n}$ are

m,n	$(a_2)_{m,n}$	$(a_1)_{m,n}$	$(a_0)_{m,n}$
1, 1	$\frac{4}{3}\mu_{00}$	$\frac{4}{3}D\mu_{00}$	$-(\mathrm{i}\alpha\rho_{00}v_{00}+\alpha^2\mu_{00})$
1, 2	0	$\frac{1}{3}\mathrm{i}\alpha\mu_{00}$	$-\frac{2}{3}\mathrm{i}\alpha D\mu_{00}$
1, 3	0	0	$\mathrm{i}\alpha\mu_{00T}Dv_{00}$
1, 4	0	-1	0
2, 1	0	$\frac{1}{3}\mathrm{i}\alpha\mu_{00}$	$\mathrm{i}\alpha D\mu_{00}-\rho_{00}Dv_{00}$
2, 2	μ_{00}	$D\mu_{00}$	$-(\mathrm{i}\alpha\rho_{00}v_{00}+\frac{4}{3}\alpha^2\mu_{00})$
2, 3	0	$\mu_{00T}Dv_{00}$	$D(\mu_{00T}Dv_{00})-Gr\rho_{00T}/(2\epsilon)$
2, 4	0	0	$-\mathrm{i}\alpha$
3, 1	0	0	$-c_{p00}\rho_{00}DT_{00}$
3, 2	0	0	0
3, 3	k_{00}/Pr	$2Dk_{00}/Pr$	$(D(k_{00T}DT_{00})-\alpha^2k_{00})/Pr-\mathrm{i}\alpha c_{p00}\rho_{00}v_{00}$
3, 4	0	0	0
4, 1	0	ρ_{00}	$D\rho_{00}$
4, 2	0	0	$\mathrm{i}\alpha\rho_{00}$
4, 3	0	0	$\mathrm{i}\alpha\rho_{00T}v_{00}$
4, 4	0	0	0

and matrix $(\mathrm{B})_{m,n}$ are

	$n=1$	2	3	4
$m=1$	ρ_{00}	0	0	0
2	0	ρ_{00}	0	0
3	0	0	$c_{p00}\rho_{00}$	0
4	0	0	$-\rho_{00}T$	0

For the specific variable properties of air we have

$$\rho_{00T} \equiv \frac{\partial\rho_{00}}{\partial T_{00}} = -\frac{P_{00}}{T_{00}^2}, \quad \mu_{00T} \equiv \frac{\partial\mu_{00}}{\partial T_{00}} = \frac{1+S_\mu}{2}\frac{T_{00}+3S_\mu}{(T_{00}+S_\mu)^2}T_{00}^{1/2},$$

$$k_{00T} \equiv \frac{\partial k_{00}}{\partial T_{00}} = \frac{1+S_k}{2}\frac{T_{00}+3S_k}{(T_{00}+S_k)^2}T_{00}^{1/2}.$$

Appendix C

Let us consider the expansion

$$w(t,x) = A(t)\,w_{11}(x) + \ldots + A(t)\,|A(t)|^2 w_{31}(x) + \ldots, \tag{C 1}$$

where $w_{11}(x)$ is an eigenfunction of the problem

$$(\boldsymbol{A}+\sigma\boldsymbol{B})\,w_{11} = 0 \tag{C 2}$$

and $w_{31}(x)$ is a solution of the problem

$$(\boldsymbol{A}+(\sigma+2\sigma^R)\,\boldsymbol{B})\,w_{31} = g(w_{11}) + K\boldsymbol{B}w_{11} \tag{C 3}$$

typically arising at the third order of the amplitude expansion (the right-hand-side g has cubic nonlinearity and K is the Landau constant to be specified). If $\sigma^R = 0$ and w_{11} is normalized as, say, $w_{11}(x_0) = 1$, then K is defined uniquely by the solvability

condition. If $\sigma^R \neq 0$, (C 3) is solvable for any K. To fix the problem, Herbert (1983) suggests introducing a *local* restriction for higher-order disturbance terms, i.e. he extends system (C 3) to

$$(\boldsymbol{A}+(\sigma+2\sigma^R)\boldsymbol{B})\,w_{31}-K\boldsymbol{B}w_{11}=g(w_{11}),\quad w_{31}(x_0)=0, \tag{C 4a, b}$$

in which case K is defined uniquely. Provided $\sigma^R K^R<0$, from the subsequent Landau equation one finds the equilibrium amplitude $|A_e|=(-\sigma^R/K^R)^{1/2}$. Subsequently, from (C 1) we have that

$$|w_e(x_0)|=(-\sigma^R/K^R)^{1/2}. \tag{C 5}$$

Let us repeat the procedure but now choosing an arbitrary $x_1 \neq x_0$ to find the new value of the Landau constant K'. Now renormalize the eigenfunction of (C 2), which we call $w'_{11}(x)$, by taking $w'_{11}(x_1)=1$ so that $w'_{11}(x)=\kappa w_{11}(x)$, where $\kappa=w_{11}(x_0)/w_{11}(x_1)$. Subsequently, the equivalent system (C 4) can be rewritten as

$$(\boldsymbol{A}+(\sigma+2\sigma^R)\boldsymbol{B})\,w'_{31}-\kappa K'\boldsymbol{B}w_{11}=\kappa|\kappa^2 g(w_{11}),\quad w'_{31}(x_1)=0. \tag{C 6a, b}$$

Furthermore, the new equilibrium amplitude is $|A'_e|=(-\sigma^R/K^{R'})^{1/2}$ and from (C 1) (now with A', w'_{11}, and w'_{31}) we have

$$|w_e(x_0)|=(-\sigma^R/K^{R'})^{1/2}\,|\kappa-(\sigma^R/K^{R'})\,w'_{31}(x_0)|. \tag{C 7}$$

For consistency with (C 5) we must have

$$\left(\frac{K^R}{K^{R'}}\right)^{1/2}\left|\kappa-\frac{\sigma^R}{K^{R'}}w'_{31}(x_0)\right|=1. \tag{C 8}$$

Unfortunately, numerical evaluations show that in general this is not true. Note also that the choice

$$K'=|\kappa|^2K,\quad w'_{31}=\kappa|\kappa|^2w_{31} \tag{C 9}$$

makes the first equation in (C 6*a*) identical with the first equation in (C 4*a*). But then it follows from (C 6*b*) that $w_{31}(x_1)=0$. Since x_1 is arbitrary, then $w_{31}\equiv 0$. Obviously, this cannot be true. The reason for this inconsistency is that Herbert proposes assessing global quantities (amplitude and Landau constant) by looking at some local characteristic (the solution at a particular point). Note that if instead of using a local property of the solution, we introduce the global condition $w_{31}\perp w_{11}$, as demonstrated in § 7, this inconsistency is completely eliminated.

REFERENCES

Benney, D. J. & Bergeron, R. F. 1969 A new class of nonlinear waves in parellel flows. *Stud. Appl. Maths* **48**, 181–204.

Benney, D. J. & Maslow, S. A. 1974 The evolution in space and time of nonlinear waves in parallel shear flows. *Stud. Appl. Maths* **54**, 181–205.

Bergholz, R. F. 1978 Instability of steady natural convection in a vertical fluid layer. *J. Fluid Mech.* **84**, 743–768.

Chen, Y.-M. & Pearlstein, A. J. 1989 Stability of free-convection flows of variable-viscosity fluids in vertical and inclined slots. *J. Fluid Mech.* **198**, 513–541.

Chenoweth, D. R. & Paolucci, S. 1985 Gas flow in vertical slots with large horizontal temperature differences. *Phys. Fluids* **28**, 2365–2374.

Chenoweth, D. R. & Paolucci, S. 1986 Natural convection in an enclosed vertical air layer with large horizontal temperature differences. *J. Fluid Mech.* **169**, 173–210.

Davey, A. & Nguyen, H. P. F. 1971 Finite-amplitude stability of pipe flow. *J. Fluid Mech.* **45**, 701–720.

DAVIS, R. E. 1969 On the high reynolds number flow over a wavy boundary. *J. Fluid Mech.* **36**, 337–346.

FUJIMURA, K. 1988 The equivalence between two perturbation methods in weakly nonlinear stability theory for parallel shear flows. *Proc. R. Soc. Lond.* A **424**, 373–392.

FUJIMURA, K. 1992*a* Addendum to 'Nonlinear equilibrium solutions for traveling waves in a free convection between vertical parallel plates'. *Eur. J. Mech.* B/*Fluids* **11**, 461–464.

FUJIMURA, K. 1992*b* Higher harmonic resonances in free convection between vertical parallel plates. *Phil. Trans. R. Soc. Lond.* A **340**, 95–130.

FUJIMURA, K. & MIZUSHIMA, J. 1987 Nonlinear interaction of disturbances in free convection between vertical parallel plates. In *Nonlinear Wave Interactions in Fluids* (ed. R. W. Miksad, T. R. Akylas & T. Herbert). AMD–Vol. 87, pp. 123–130. ASME.

FUJIMURA, K. & MIZUSHIMA, J. 1991 Nonlinear equilibrium solutions for traveling waves in a free convection between vertical parallel plates. *Eur. J. Mech.* B/*Fluids* **10**, 25–30.

FUKUI, K., NAKAJIMA, M., UEDA, H., SUZAKI, K. & MIZUSHINA, T. 1982 Flow instability and transport phenomena in combined free and forced convection between vertical parallel plates. *J. Chem. Engng Japan* **15**, 172–180.

GOTOH, K. & IKEDA, N. 1972 Secondary convection in a fluid between parallel vertical plates of different temperatures. *J. Phys. Soc. Japan* **33**, 1697–1705.

GUCKENHEIMER, J. & HOLMES, P. J. 1983 *Nonlinear Oscillations, Dynamical Systems, and Bifurcations of Vector Fields*, Chapter 7.5. Springer.

HABERMAN, R. 1972 Critical layers in parallel flows. *Stud. Appl. Maths* **51**, 139–161.

HERBERT, T. 1983 On perturbation methods in nonlinear stability theory. *J. Fluid Mech.* **126**, 167–186.

IMSL, INC. 1989 *IMSL Mathematical Library, Version 1.1*. Houston, TX.

LEE, Y. & KORPELA, S. A. 1983 Multicellular natural convection in a vertical slot. *J. Fluid Mech.* **126**, 91–121.

MACSYMA, INC. 1995 *Macsyma – Mathematics and System Reference Manual*, 15th edn. Arlington, MA.

MIZUSHIMA, J. 1990 Equilibrium solution of the secondary convection in a vertical fluid layer between two parallel plates. *Fluid Dyn. Res.* **5**, 289–299.

MIZUSHIMA, J. & GOTOH, K. 1983 Nonlinear evolution of the disturbance in a natural convection induced in a vertical fluid layer. *J. Phys. Soc. Japan* **52**, 1206–1214.

MIZUSHIMA, J. & SAITO, Y. 1987 Equilibrium characteristics of the secondary convection in a vertical fluid layer between two flat plates. *Fluid Dyn. Res.* **2**, 183–191.

PAOLUCCI, S. 1982. On the filtering of sound from the Navier–Stokes equations. *Tech. Rep.* SAND82-8257. Sandia National Laboratories, Livermore, California.

STEWARTSON, K. & STUART, J. T. 1971 A non-linear instability theory for a wave system in plane Poiseuille flow. *J. Fluid Mech.* **48**, 529–545.

STUART, J. T. 1960 On the non-linear mechanics of wave disturbances in stable and unstable parallel flows. Part 1. The basic behaviour in plane Poiseuille flow. *J. Fluid Mech.* **9**, 353–370.

SUSLOV, S. A. 1997 Nonlinear analysis of non-Boussinesq convection. PhD thesis, University of Notre Dame, USA.

SUSLOV, S. A. & PAOLUCCI, S. 1995*a* Stability of natural convection flow in a tall vertical enclosure under non-Boussinesq conditions. *Intl J. Heat Mass Transfer* **38**, 2143–2157.

SUSLOV, S. A. & PAOLUCCI, S. 1995*b* Stability of mixed-convection flow in a tall vertical channel under non-Boussinesq conditions. *J. Fluid Mech.* **302**, 91–115.

WATSON, J. 1960 On the non-linear mechanics of wave disturbances in stable and unstable parallel flows. Part 2. The development of a solution for plane Poiseuille flow and for plane Couette flow. *J. Fluid Mech.* **9**, 371–389.

WHITE, F. M. 1974 *Viscous Fluid Flow*. McGraw-Hill.